J Neurophysiol 118: 2789–2805, 2017.
First published August 9, 2017; doi:10.1152/jn.00253.2017.

RESEARCH ARTICLE | *Higher Neural Functions and Behavior*

Sequential hemifield gating of α- and β-behavioral performance oscillations after microsaccades

Joachim Bellet,[1,2,3] Chih-Yang Chen,[1,2,3] and Ziad M. Hafed[1,3]

[1]*Werner Reichardt Centre for Integrative Neuroscience, Tuebingen University, Tuebingen, Germany;* [2]*Graduate School of Neural and Behavioural Sciences, International Max Planck Research School, Tuebingen University, Tuebingen, Germany; and* [3]*Hertie Institute for Clinical Brain Research, Tuebingen University, Tuebingen, Germany*

Submitted 5 April 2017; accepted in final form 8 August 2017

Bellet J, Chen CY, Hafed ZM. Sequential hemifield gating of α- and β-behavioral performance oscillations after microsaccades. *J Neurophysiol* 118: 2789–2805, 2017. First published August 9, 2017; doi:10.1152/jn.00253.2017.—Microsaccades are tiny saccades that occur during gaze fixation. Even though visual processing has been shown to be strongly modulated close to the time of microsaccades, both at central and peripheral eccentricities, it is not clear how these eye movements might influence longer term fluctuations in brain activity and behavior. Here we found that visual processing is significantly affected and, in a rhythmic manner, even several hundreds of milliseconds after a microsaccade. Human visual detection efficiency, as measured by reaction time, exhibited coherent rhythmic oscillations in the α- and β-frequency bands for up to ~650–700 ms after a microsaccade. Surprisingly, the oscillations were sequentially pulsed across visual hemifields relative to microsaccade direction, first occurring in the same hemifield as the movement vector for ~400 ms and then the opposite. Such pulsing also affected perceptual detection performance. Our results suggest that visual processing is subject to long-lasting oscillations that are phase locked to microsaccade generation, and that these oscillations are dependent on microsaccade direction.

NEW & NOTEWORTHY We investigated long-term microsaccadic influences on visual processing and found rhythmic oscillations in behavioral performance at α- and β-frequencies (~8–20 Hz). These oscillations were pulsed at a much lower frequency across visual hemifields, first occurring in the same hemifield as the microsaccade direction vector for ~400 ms before switching to the opposite hemifield for a similar interval. Our results suggest that saccades temporally organize visual processing and that such organization can sequentially switch hemifields.

microsaccades; fixational eye movements; α-rhythms; β-rhythms; perceptual oscillations

MICROSACCADES ARE SMALL SACCADES that occur during gaze fixation (Cherici et al. 2012; Hafed et al. 2015; Krauzlis et al. 2017; Poletti and Rucci 2016). These eye movements are governed by similar brain generation mechanisms as larger saccades (Goffart et al. 2012; Hafed 2011; Hafed et al. 2009; Hafed and Krauzlis 2012; Peel et al. 2016; Zuber et al. 1965), suggesting a precise level of control over the metrics and kinematics of these movements (Buonocore et al. 2017; Guerrasio et al. 2010; Havermann et al. 2014; Ko et al. 2010; Poletti et al. 2013; Tian et al. 2016). Interestingly, despite their small size, microsaccades are also associated with substantial modulations in neural activity and behavior and over a wide range of retinal eccentricities all the way from the fovea to the periphery (Bosman et al. 2009; Chen and Hafed 2017; Chen et al. 2015; Hafed 2013; Hafed et al. 2015; Hafed and Krauzlis 2010; Herrington et al. 2009; Tian et al. 2016; Zuber and Stark 1966). Such perimicrosaccadic modulations can be quite strong. For example, suppression of visual sensitivity for stimuli presented around the time of microsaccades can reach levels of ~50% in structures like the superior colliculus (SC) and lasts for ~100 ms after movement onset (Chen and Hafed 2017; Chen et al. 2015; Hafed and Krauzlis 2010). Moreover, perimicrosaccadic changes in vision result in performance changes that are virtually identical to those in a variety of experiments involving "covert" processing without eye movements (Chen et al. 2015; Hafed 2013; Hafed et al. 2015; Tian et al. 2016). Therefore, understanding the relationships between microsaccades and visual performance not only can enrich the microsaccadic literature itself but also can potentially illuminate findings in other related topics in perception and cognition.

The majority of studies of perimicrosaccadic modulations in vision so far have focused on a tight temporal window of ~50–100 ms around microsaccade onset. Since microsaccades are driven by saccade motor control circuitry (Hafed et al. 2009; Hafed and Krauzlis 2012; Peel et al. 2016), and since they also refresh retinal images (Martinez-Conde et al. 2000), it is reasonable to expect that changes in visual representations would occur during such a tight temporal window (Hafed et al. 2015; Krauzlis et al. 2017). However, microsaccades may also be associated with longer term changes in brain state going beyond simple "transient recovery."

In this study, we specifically hypothesized that microsaccades globally reset the visual system, meaning that after "transient recovery," the brain does not return to a random state but to a coherently structured steady-state oscillatory pattern. Such a pattern is so coherent and reliable across individuals that it manifests in alterations of the visual system's efficiency in detecting stimuli even at the behavioral level and even up to several hundreds of milliseconds after microsaccades. In this regard, we were motivated by findings of synchronization of endogenous brain rhythm behavioral manifestations with mo-

Address for reprint requests and other correspondence: Z. M. Hafed, Werner Reichardt Centre for Integrative Neuroscience, Otfried-Mueller Str. 25, Tuebingen 72076, Germany (e-mail: ziad.m.hafed@cin.uni-tuebingen.de).

tor actions. For example, Benedetto and colleagues have recently found a synchronous relationship between ~3.5- and 8-Hz behavioral oscillation rhythms of contrast sensitivity and reaching arm movements (Benedetto et al. 2016; Tomassini et al. 2015). Moreover, large, voluntary saccades are associated with phase locking of ~3- to 4-Hz behavioral oscillations (Benedetto and Morrone 2017; Hogendoorn 2016; Wutz et al. 2016), and microsaccades have been shown to reset physiological α rhythms (~10 Hz) in occipital cortex (Gaarder et al. 1966).

In our experiments, we therefore explored both time-dependent and microsaccade-direction-dependent long-term behavioral fluctuations after the occurrence of microsaccades. Unlike in the large-saccade literature (Benedetto and Morrone 2017; Hogendoorn 2016; Wutz et al. 2016), we observed higher frequency oscillations in the α- and β-frequency ranges. This is interesting as it might relate to findings of higher frequency behavioral oscillations in attentional state (Song et al. 2014), which is known to be correlated with microsaccades (Engbert and Kliegl 2003; Hafed 2013; Hafed and Clark 2002; Hafed et al. 2011; 2013; Kliegl et al. 2009; Laubrock et al. 2005; Peel et al. 2016; Tian et al. 2016).

As we will show, our results demonstrate that visual processing is almost never exempt from saccade-related influences, highlighting the importance of adopting an "active perception" approach to vision science.

MATERIALS AND METHODS

We performed two behavioral experiments on human subjects, and we also analyzed neurophysiological data from the SC of two male rhesus macaque monkeys (*Macaca mulatta*, aged 7 yr). As we describe below, the logic of all experiments was to present stimuli after microsaccade occurrence and to measure either behavioral or neural responses to these stimuli, with the specific goal of probing longer times after microsaccade onset than we had previously explored (Chen and Hafed 2017; Chen et al. 2015; Hafed 2013; Hafed et al. 2015; Hafed and Krauzlis 2010).

Ethics committees at Tuebingen University approved the human experiments, and human subjects provided informed, written consent in accordance with the Declaration of Helsinki. Monkey experiments were approved by the regional governmental offices of the city of Tuebingen.

Behavioral Tasks

Experiment 1: reaction time task. Human subjects sat in a dark room facing a computer display (41 pixels/°; 85 Hz). Head fixation was achieved through a custom-made chin/forehead rest (Hafed 2013), and we measured eye movements using a video-based eye tracker (EyeLink 1000; SR Research). In each trial, a white fixation spot (6-min arc in diameter; 89.1 cd/m^2) appeared on a gray screen (22.3 cd/m^2) (Fig. 1*A*). After a random time, a target (white circle subtending 1° in diameter) appeared at 5° either to the right or left of fixation, and the fixation spot disappeared. Subjects were instructed to execute a saccade as fast as possible to the target. Unbeknownst to the subjects, they continuously made microsaccades during fixation, and our experimental goal was to investigate reaction time (RT) to the target as a function of when this target appeared after a given microsaccade (Fig. 1*A*). We wanted to sample as long an interval as possible between a given microsaccade and target onset, such that we could uncover long-term microsaccadic effects on RT. As a result, and for the first six subjects who took part in the experiment, we programmed the experiment such that the target could appear between 1,000 and 3,000 ms after the initial fixation spot onset. The idea behind using such a long interval was to increase our chances of having trials with a very long delay between a microsaccade and target onset (i.e., to obtain long time courses of RT fluctuations; e.g., see Fig. 3*A* in RESULTS). Specifically, since intermicrosaccadic intervals can be short (e.g., see Fig. 4*B* in RESULTS), we needed to have sufficient trials with long delays to be able to sample enough cases in which no intervening microsaccades occurred for a long time after a given movement until target onset. Having said that, and to accelerate data collection, we found that we could shorten trial lengths for the last four subjects that we recruited; in this case, the target could appear between 300 and 1,300 ms after fixation spot onset. Even in these cases, we ensured that our data analyses included only microsaccades occurring after >300 ms of steady fixation (for reasons clarified below).

We collected data from 10 subjects (6 females; 2 authors; 22–39 yr old). All subjects completed 5 sessions of 1 h each, and we analyzed a total of 10,817 trials in this experiment. As stated above, this large number of trials was needed to allow us to sample enough time points after individual microsaccades. In reality, for any given time bin in our analyses, the number of trials used was much less than the total number of trials collected (e.g., see Fig. 3*A* in RESULTS).

Experiment 2: perceptual detection task. In a second experiment, we collected data from 14 human subjects (9 females; 2 authors; 22–39 yr old), and all subjects completed 3–5 sessions of 1 h each.

Each trial started with the appearance of a black fixation spot subtending a 6-min arc in diameter along with white vertical lines (3-min arc × 4°) that were vertically centered 3° above and below the two probable horizontal locations of an upcoming target (Fig. 1*B*). The target was a dot subtending a 4-min arc in diameter presented horizontally 5° to the right or left of fixation. The target was presented only briefly for ~12 ms. The luminance of the target was darker than the background, and it was continuously adjusted from trial to trial with a staircase procedure (see below) to maintain correct target detection performance of ~50% throughout all sessions. In our design, "correct target detection" meant that subjects reported both a conscious percept of the target and its correct location, because they also always had the option to report "target not seen" (see below). We chose to continuously adjust task difficulty to maintain ~50% correct detections to demonstrate the robustness of our observed modulations in target detection likelihoods at different times after microsaccades (e.g., see Fig. 7 in RESULTS) and also to ensure stable performance in the face of fluctuations in subject arousal during the sessions. This has also allowed us to combine subjects in analyses, as we describe below.

The target was presented at a random time ranging from ~61 to ~1,061 ms after gaze entered a virtual window of 2° radius around the fixation spot. Subjects were instructed to press a button corresponding to the target location (right or left) as soon as it was consciously seen (Fig. 1*B*). Because the target was difficult to see, we presented a question mark at screen center 500–700 ms after target presentation to indicate to subjects that they needed to make a response (Fig. 1*B*). When the question mark was visible, subjects could either press a middle button to indicate that the target was not seen or to press the button corresponding to the right/left target location if it was seen. Subjects were instructed not to guess the location and to only answer when the target was consciously seen. To ensure that the subjects followed the task instructions, 10% of the trials were designated as catch trials with no target appearing at all, and we confirmed that false alarms on these catch trials were much less frequent than correct detections; we also confirmed that erroneous localizations of the target when subjects reported consciously seeing it were rare (e.g., see Fig. 7*A* in RESULTS). Auditory feedback signaled if target localization was correct or not. There was no auditory feedback when the subjects reported not seeing the target.

For each subject, the first session in this experiment was used solely to estimate target contrast needed to achieve ~50% correct target detections. The luminance of the target was first started at background

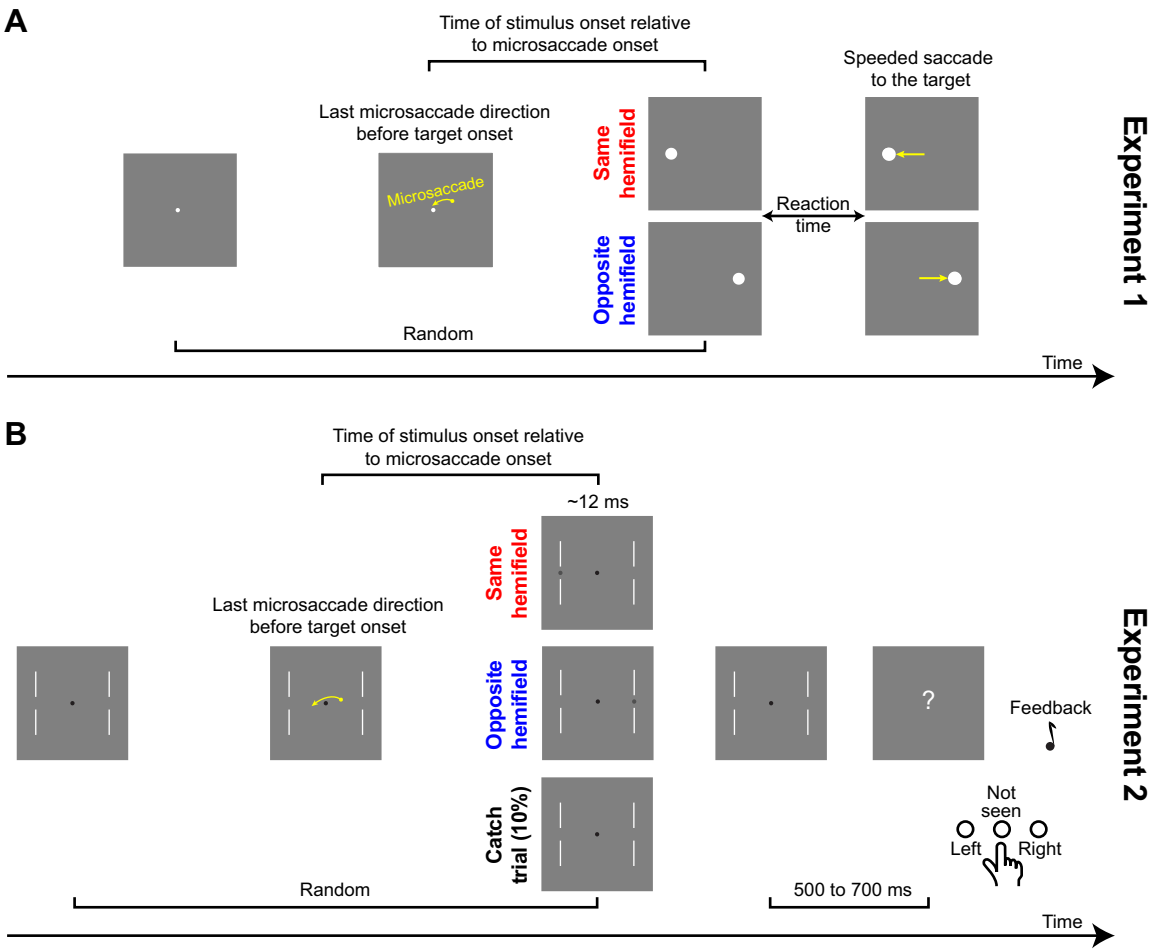

Fig. 1. Behavioral tasks. *A*: *experiment 1*. Subjects generated a target-directed saccade. Before target onset, subjects could generate a microsaccade either toward the same or opposite hemifield as the target. We analyzed reaction time (RT) as a function of target onset time and direction relative to microsaccades, and we ensured that there were no intervening movements (saccades or microsaccades) or blinks between the microsaccade of interest and target onset. *B*: *experiment 2*. Subjects detected a target at threshold by indicating its location (or that they did not see any target). Task difficulty was continuously adjusted to keep conscious target detections at ~50% (see MATERIALS AND METHODS).

contrast, which meant that subjects could not detect the target. After every "target not seen" response by the subjects (Fig. 1*B*), the luminance of the target was stepped by one display-gun value on our eight-bit display driver (i.e., 1 out of 256 levels). As soon as the target began to be detected, we started a procedure of monitoring correct target detections based on the previous 50 trials. Target luminance was increased or decreased by 1 display-gun value if average performance was above 66% or below 34%, respectively, during the previous 50 trials. For the subsequent sessions, target luminance started at the level predicted from the first session, and it was continuously adjusted (always based on performance in the previous 50 trials) using the same incremental procedure. This approach enabled us to track the ~50% threshold well (e.g., see Fig. 8*A* in RESULTS). We analyzed a total of 6,693 trials from this task.

Experiment 3: monkey SC recordings. We performed a novel analysis on data that were part of the set used to describe a previous report (Chen et al. 2015); here, we critically extended our analysis window as long as possible after microsaccade onset to explicitly sample longer time courses of neural modulations of SC visual sensitivity after microsaccades than were analyzed in the previous report. Briefly, two monkeys fixated, and we presented a 2.2 cycles/° vertical sine wave grating in a neuron's visual response field. The grating was tailored in size to the response field size, and we varied the contrast from trial to trial. We considered as "baseline" visual response the response of SC neurons when the grating appeared with no microsaccades occurring within ±150 ms from grating onset. We then measured the visual response of the same neurons when the grating appeared at a given time after a microsaccade. Once again, the difference in the present study from our earlier experiments was that we increased the time window of analysis as much as possible (see Fig. 10 in RESULTS).

Data Analysis

Microsaccades and saccades were detected offline using velocity and acceleration criteria (Chen and Hafed 2013), and microsaccade misdetections were checked manually for all trials. We defined as microsaccades all fixational saccades with amplitudes $<1°$; in reality, median amplitude was a 14.6-min arc in *experiment 1* and a 17.6-min arc in *experiment 2*.

Since we observed that microsaccade frequency increased substantially in the first 300 ms following fixation spot onset (e.g., see Fig. 4*C* in RESULTS), we only analyzed trials in which the last microsaccade to occur before target onset actually occurred >300 ms after fixation spot onset. This was done to ensure that the phase locking that we observed in this study (see RESULTS) was to microsaccades and not necessarily to another resetting event (i.e., fixation spot onset). In a control analysis, we also analyzed data when target onset time was measured with respect to fixation spot onset and not to microsaccade onset; in this case, it was irrelevant whether or not a microsaccade had occurred between fixation spot onset and target onset.

Experiment 1: RT task. Our goal in this experiment was to analyze the spectrotemporal variation of RT as a function of when a target appeared after a given microsaccade (Fig. 1*A*). We thus performed a series of analysis steps that are graphically illustrated in Fig. 2 on an example artificial data set designed to clarify our procedures as much as possible (real data are presented in all subsequent figures). In what follows, we step through the details of our analyses with the aid of this figure.

We first excluded the 2.5% fastest and 2.5% slowest RTs of each subject from any further analysis. We then demeaned each subject's RT distribution by obtaining RT values expressed as a difference from the overall mean RT, thus reducing intersubject variability. We then pooled trials from all subjects together, similar to what has been done previously (Hogendoorn 2016), and we plotted RT as a function of when a target on a given trial appeared after a microsaccade (also see below for further justification). This resulted in a scatter plot similar to that shown in Fig. 2*A*, *top*. The mean RT value per subject was obtained from all trials regardless of when microsaccades or target onsets occurred. Also, in every trial, the demeaned RT value was plotted as a function of the time of target appearance relative to microsaccade onset for the very last microsaccade to occur before target onset (Fig. 1*A*), such that we ensured that there were no intervening microsaccades (or other eye movements) between the microsaccade of interest and the target onset. This means that if there were multiple microsaccades during the fixation period before target onset (a rarity), the time interval of interest to us was the time between target onset and the final microsaccade to occur before such onset. We also excluded any trials with blinks between the microsaccade of interest and target onset.

To obtain the time course of RT fluctuations, we computed the mean value across all trials using a running window of 50 ms in width in steps of 1 ms (Fig. 2*B*, *top*). Note that such a running window is

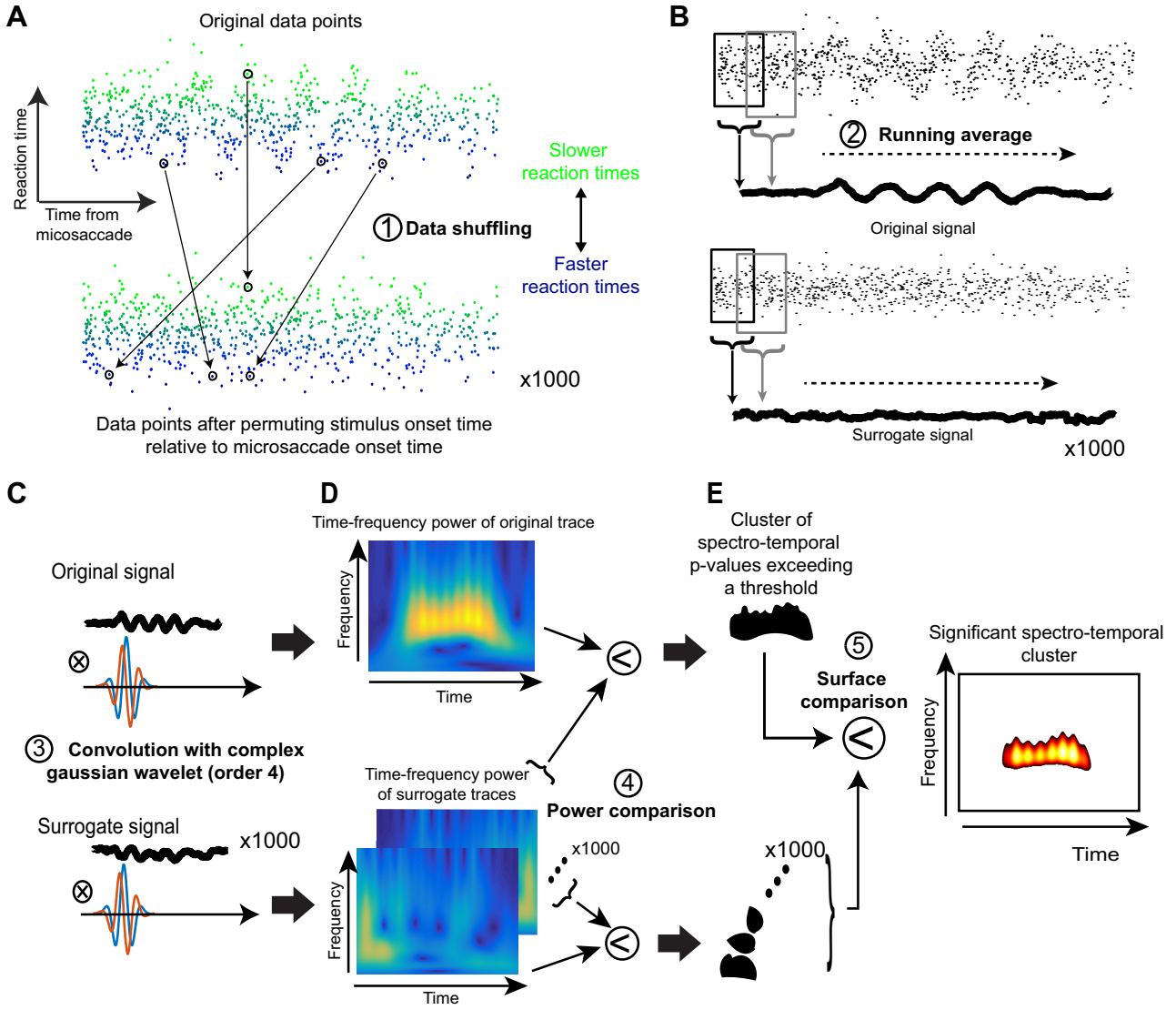

Fig. 2. Steps used for time-frequency analyses in our study. *A*: we collected all trials and plotted each trial's RT (as in the case of *experiment 1*) as a function of target onset time relative to a microsaccade. In this illustrative example, we show artificial data that have an underlying oscillatory pulse embedded in noise. *Bottom*: we shuffled the data in time, and we did this 1,000 times to obtain 1,000 surrogate data sets. *B*: we filtered the data using a running average to obtain a time course of fluctuations in the real data (*top*) and also for each of the 1,000 surrogate data sets. *C*: we then convolved each of the time course traces with a complex Gaussian wavelet of order 4. *D*: this allowed us to obtain time-frequency power spectra. For the real data, high power was observed during the interval in which an oscillation pulse was present in the original signal. The surrogate data sets had high power at random places in the time-frequency plots. *E*: we established statistical significance, with corrections for multiple comparisons, by finding a cluster in 2-dimensional time-frequency space in the original data set that was unlikely to be observed by chance from similar clusters observed in the surrogate data sets. We then plotted this "outlying" cluster with its associated *P* values as the significant cluster of spectrotemporal oscillation.

equivalent to implementing a 20-Hz low-pass filter, and it reduces the amplitude of oscillations. The higher in frequency an oscillation is (and approaching 20 Hz), the more its amplitude will be reduced by the running window analysis. This also means that our analyses could not detect oscillations higher than 20 Hz in frequency; however, to our knowledge, behavioral oscillations are rarely studied above this frequency. For some analyses (e.g., see Fig. 5 in RESULTS), we performed this same RT time-course analysis but only for trials in which the target appeared either in the "same" hemifield as the microsaccade direction vector or in the "opposite" hemifield. In addition, in yet other analyses (e.g., see Figs. 3 and 5 in RESULTS), we also computed the RT time courses for only microsaccades smaller than a 30-min arc in amplitude.

To obtain the spectral content of RT fluctuations, we analyzed the RT time course in the interval 100–800 ms after microsaccade onset (Fig. 2, *A* and *B*). We excluded the first 100 ms after microsaccade onset because this period is dominated by "microsaccadic suppression" effects on RT (Chen and Hafed 2017; Chen et al. 2015; Hafed et al. 2015; Hafed and Krauzlis 2010; Tian et al. 2016), as we detail in RESULTS. We first removed the slow fluctuation trend of the signal (any <2-Hz fluctuation) by using a finite impulse response low-pass filter (Fieldtrip Toolbox; Oostenveld et al. 2011) and subtracting the result from the original curve (Fig. 2*B*, *top*). The detrended signal was then transformed using continuous complex Gaussian wavelets (order 4) for frequencies ranging from 2 to 20 Hz in steps of 0.25 Hz (Fig. 2*C*, *top*). The power of the resulting time-frequency image was defined as the square of the absolute value of the complex transform (Fig. 2*D*, *top*). We now had a time-frequency plot of spectrotemporal variation in RT (Fig. 2*D*, *top*).

To assess statistical significance of given time intervals and/or frequency bands in the spectral analysis, we used the following starting point: the hypothesis in this study was that the oscillations that we observed in RT were caused by the time at which a stimulus was presented relative to a microsaccade (see RESULTS). In other words, such oscillations can hardly ever be observed if we were to compose surrogate signals by randomly arranging the behavioral responses in time (i.e., without regard to the real time of stimulus onset relative to a microsaccade; Fig. 2*A*, *bottom*). We therefore tested the probability that random permutations in the *x*-label values of figures like Fig. 2*A*, *top*, would result in as much as or more spectral power than the original data. To generate a statistic, the following procedure was repeated 1,000 times. We used data points that were collected outside the microsaccadic suppression period (i.e., >100 ms after microsaccade onset), and we arranged them randomly relative to the time of a virtual microsaccade (Fig. 2*A*, *bottom*). Care was taken such that there were as many data points assigned for each time point as in the original measurements, such that the difference in power between original signals and surrogate signals could not be explained by differences in variability (Fig. 2*A*). The randomly arranged data points were then processed using the exact same procedures as the original data: time courses were obtained using running windows (Fig. 2*B*, *bottom*); time courses were detrended; and finally, time courses were wavelet-transformed (Fig. 2, *C* and *D*, *bottom*). For each time-frequency point in the original power spectrum, *P* values were defined as the proportion of power spectra in surrogate data that led to an equal or higher power than the original data (Fig. 2*E*). $P < 0.05$ was considered as significant. To control for multiple comparisons, we additionally used a nonparametric statistical test of the size of the cluster of adjoining significant *P* values (Maris and Oostenveld 2007). More specifically, the multiple comparisons test consisted of determining the probability of obtaining a cluster (defined as a 2-dimensional region in time-frequency space) of adjoining significant *P* values as big as or bigger than the one obtained with the original data. To this end, each of the 1,000 power spectra obtained by random permutations was compared with the 999 other random power spectra (Fig. 2*D*, *bottom*). This resulted in 1,000 sets of *P* values. Clusters of significant *P* values from the original power spectrum passed the multiple comparisons test if their size was >95% of the biggest clusters of adjoining significant *P* value in each randomly drawn set of *P* values (Fig. 2*E*).

Our approach to statistical tests of the oscillations provided us with the most conservative estimates of significant oscillations in our data. This was important because using a running window (i.e., a low-pass filter) can cause ringing in signals that may erroneously appear like oscillations by visual inspection. For example, see Figs. 3*B* and 5, *B* and *E*, in RESULTS for examples of surrogate traces from our analyses after the shuffling step of Fig. 2*A*. In some of these sample shuffled traces, visual inspection might lead one to assume that an oscillation was present. Thus our approach was to err on the conservative side to be certain that our interpretations of oscillations are highly reliable. This is also why we additionally ensured using similar numbers of data points in each time bin in our shuffled signals as in the real data.

To rule out the possibility that RT oscillations may have resulted from an increase of variance in RT after microsaccade onset, for example, as suggested in (Zoefel and Sokoliuk 2014), we investigated whether the phase of RT oscillation time courses was consistent across subjects. To represent the instantaneous phase of oscillations in each subject (e.g., see Fig. 6), we first obtained individual time courses of RT using an averaging running window of 50 ms in the "same hemifield" condition (i.e., when the target appeared in the same hemifield as a microsaccade direction vector). In the "opposite hemifield" condition, we chose a 78-ms averaging window instead to obtain the best estimate of the phase of α-oscillations in each subject (because "opposite" oscillations were lower in frequency than "same" oscillations, as we show in RESULTS). We then band-passed the traces in the frequency bands of interest based on Fig. 5 (13–20 Hz in the same condition and 8–12 Hz in the opposite condition; see RESULTS), and we extracted the instantaneous phase with a Hilbert transform (see Fig. 6 in RESULTS). Even though such a transform, which is well established to evaluate phase (Le Van Quyen et al. 2001), may introduce phase distortions at the edges of a signal interval, such distortions would also occur in permuted data during significance testing (see below); thus, if anything, there may be more false negatives at the edges of an interval being analyzed. To quantify the instantaneous phase consistency between subjects, we calculated the phase-locking value (PLV) at each time point after microsaccade onset:

$$PLV = \frac{1}{n} \cdot \left| \sum_{k=1}^{n} e^{i\theta_k[2\pi]} \right| \quad (1)$$

where n is the number of subjects and θ_k the instantaneous phase from the k^{th} subject. The PLV is between 0 (no coherence) and 1 (complete coherence) (Lachaux et al. 1999).

We assessed the statistical significance of an increased PLV by using random permutations (e.g., Fig. 2*A*) and cluster corrections for multiple comparisons. The PLV was computed for 1,000 sets of 10 surrogate signals (1 per subject). A *P* value for each time bin was obtained by comparing the original PLV traces to the surrogate ones. We also obtained surrogate *P* values by comparing each surrogate PLV trace to the 999 other traces. We then measured the size of the clusters of adjoining *P* values from the original PLV trace that were <0.1. This threshold was meant to reveal long-lasting PLV increases, but the exact choice does not affect the false alarm rate of the statistical test (Maris and Oostenveld 2007). We tested the probability that clusters obtained from surrogate *P* values below the threshold had a size equal to or exceeding the size of the cluster from the original signal. If <5% of the biggest clusters from each of the 1,000 surrogate *P* value traces were bigger than the cluster from the original signal, then the whole period of increased PLV was considered as significant.

Finally, we also performed discrete Fourier transform (DFT) analysis on RT fluctuations in the interval 100–400 ms after microsaccade onset (i.e., the interval in which we observed significant oscillations throughout the different conditions; see RESULTS). We assessed signif-

icance of individual frequency ranges using a similar approach to that described above (including multiple comparison corrections), except that there was now only one dimension to work with (i.e., frequency) as opposed to two (i.e., time and frequency). We also performed such DFT analysis for microsaccades either smaller than or larger than the median amplitude.

It should be noted once again here that we combined all trials from all subjects in most of our analyses, as in Hogendoorn (2016). Given that our subjects performed similar numbers of trials to each other, it was unlikely that our results could be dominated entirely by only a subset of outlying subjects, and so our choice was justified. We also confirmed this by our PLV analyses described above, because such analyses can reveal phase consistency across individuals, and we took measures in all of our statistical analyses to take the varying numbers of observations per time bin into account. If each subject's data were first grouped into a single average trace before averaging across subjects, as performed in some other studies, such information about variability of numbers of observations per time bin would have been lost, which in turn increases the likelihood that outlying subjects may have distorted the measured signal-to-noise ratios in the averages.

Experiment 2: perceptual detection task. We used a similar time-course analysis on detectability as a function of time of target appearance relative to a microsaccade. Specifically, we computed the proportion of detected targets combining data points from all subjects together with a running window of 50 ms in width. We also used the same spectral analyses on these time courses as in the RT task described above and illustrated in Fig. 2. We should emphasize here that our task was not a classic two-alternative forced choice task. Thus, by "proportion of correct target detections," we mean the fraction of noncatch trials in which subjects reported seeing the target and correctly localized it. Thus, if this proportion was 50% (as per task design), then this means that the remaining 50% of the trials could be of two types: *1*) either subjects indicated "target not seen" in their response (which was the great majority of cases; see RESULTS); or *2*) subjects erroneously reported seeing the target in the wrong location. This also means that microsaccadic suppression alluded to above can lead to reductions in "correct target detections" to levels well below 50%, as we show in RESULTS.

To assess the statistical reliability of the difference in perceptual detection performance between two conditions (e.g., "same" vs. "opposite" or "close" vs. "far"; see Fig. 7), we used two-proportion *z*-tests.

To study the effects of microsaccade directions while canceling out the influence of gaze distance to the target (or equivalently, retinotopic target position relative to the fovea) at the time of target onset, we downsampled the data sets such that the distribution of retinotopic target positions was the same whether the target appeared in the same or opposite hemifield from a microsaccade. Specifically, we split the entire distribution of observed retinotopic target positions into 50 quantiles. Then, within each quantile, we had a distribution of N "same" trials and a distribution of M "opposite" trials. If N was larger than M, we randomly picked M trials from the "same" distribution to match the numbers of trials in the quantile to the "opposite" distribution; similarly, if M was larger than N, we randomly picked N trials from the "opposite" distribution. This resulted in matched distributions of retinotopic target positions between same and opposite trials. From these matched distributions, we compared detection performance on same vs. opposite trials, and we also measured detection performance from the same data after shuffling the "same" and "opposite" labels (to obtain a surrogate data set). Since this downsampling procedure required randomly selecting subsets of data, we repeated this procedure 1,000 times, obtaining 1,000 downsampled distributions and also 1,000 surrogate measurements from shuffled data. The *P* value was calculated as the likelihood of observing differences between "same" and "opposite" shuffled data sets that were larger in absolute value than the differences in performance between the real "same" and "opposite" conditions observed with overlapping retinotopic target positions.

We also compared detection performance on same vs. opposite microsaccade trials to detection performance on "close" vs. "far" trials. We repeated the same comparison of perceptual detection performance but after labeling trials as either having "close" or "far" target positions relative to the fovea instead of being from "same" or "opposite" microsaccade trials. To obtain "close" and "far" trials, we performed a median split on the Euclidean distance between gaze and the target (see Fig. 7*B*, *right*). In other words, in this analysis, we simply asked whether any changes in perceptual detection performance between same and opposite microsaccade trials were in reality caused by the potential that retinotopic target position relative to the fovea altered visual acuity and therefore detection performance (see RESULTS). Finally, to explore whether there were different effects for different microsaccade sizes, we repeated the comparisons between "same" and "opposite" trials but only for trials in which microsaccades were either less than a 30-min arc in amplitude or when they were classified as being larger or smaller than the median amplitude.

Experiment 3: monkey SC recordings. We repeated the time course analyses described in detail in (Hafed and Krauzlis 2010), but we extended them in time as much as possible given the data set available. We combined trials from 20, 40, and 80% contrast because these trials consistently exhibited robust visual responses. We normalized responses to the "baseline" of each contrast individually to ensure that our plots of neural fluctuations (e.g., see Fig. 10) isolate the influence of microsaccades on visual response strength, independent of stimulus contrast. As stated above, we considered as "baseline" neural responses those responses that were observed when stimuli appeared without any microsaccades occurring within ±150 ms from stimulus onset.

RESULTS

Microsaccades Reset the Phase of α- and β-Frequency Oscillatory RT Fluctuations

In *experiment 1*, we analyzed visual processing efficiency by asking 10 human subjects to perform a speeded RT task. Subjects fixated on a spot, and we then presented a bright target at 5° eccentricity either to the right or left of fixation (Fig. 1*A*, see MATERIALS AND METHODS). Subjects had to look at the target as fast as possible, and we investigated RT modulations as a function of when the target appeared relative to a microsaccade. This task has previously been shown to provide a very sensitive behavioral measure of visual sensitivity changes of SC neurons around microsaccades (Chen and Hafed 2017; Hafed and Krauzlis 2010). The key here was to densely sample many times even long after movement occurrence. We measured RT for stimuli appearing up to 800 ms after a given movement, and we took care to ensure that there were no other microsaccades, saccades, or blinks occurring between the microsaccade of interest and the target (see MATERIALS AND METHODS). We also aimed to identify only common effects across individuals. We thus subtracted each subject's overall mean RT from each trial's measurement, obtaining a differential RT value, and we then combined trials from all subjects in analyses.

When the target appeared immediately after a microsaccade, we observed an expected RT cost (Chen and Hafed 2017; Chen et al. 2015; Hafed and Krauzlis 2010). Specifically, Fig. 3*A*, *top*, shows a plot of differential RT value across subjects as a function of target onset time after a microsaccade. The error bars in Fig. 3 show SE values across all trials from all subjects combined (see MATERIALS AND METHODS), and Fig. 3*A*, *bottom*,

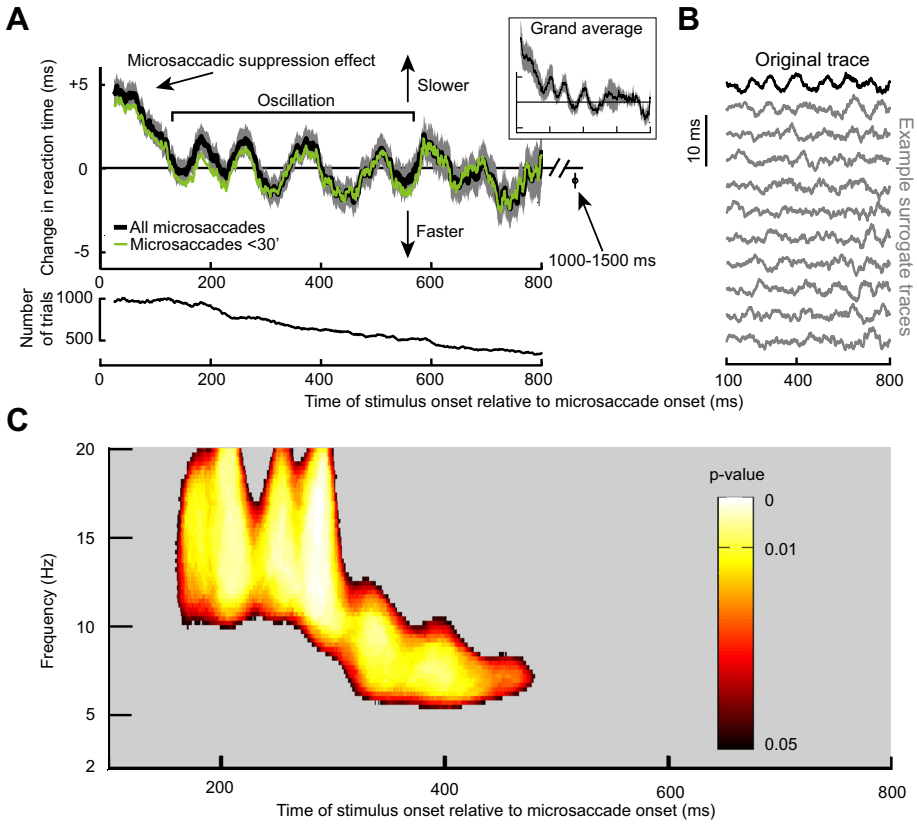

Fig. 3. Long-term microsaccadic influence on RT. *A*: change in mean RT as a function of target onset time relative to a microsaccade. This trace shows the demeaned RT trace before detrending (see MATERIALS AND METHODS). After an initial ~100-ms period of RT costs (i.e., increases) due to "microsaccadic suppression," RT oscillated coherently for almost 600 ms. Error bars denote SE across all trials from all subjects combined (see MATERIALS AND METHODS), and we used a running window of 50 ms (in steps of 1 ms); the *inset* shows that we obtained very similar RT fluctuations when individual subject data were first averaged into a single subject trace and then all the single subject traces averaged together to obtain a grand average. The *bottom* shows the number of trials used per time bin in the *top* and using the same running window procedure. Also, the green trace shows results from only trials with microsaccades less than a 30-min arc in amplitude. Note that the RT oscillation (and subsequent measurement for 1,000–1,500 ms shown as an individual data point) hovered slightly below 0. This is because the total average used to demean RT included all trials even those with target onset <300 ms from fixation spot onset; because these early trials almost always had a microsaccade (e.g., Fig. 4*C*), they had long RTs due to microsaccadic suppression, and this elevated the average RT value slightly. *B*: the *top trace* in black is the original demeaned and detrended RT trace from the same data in *A*. Below this trace are 10 example surrogate traces according to the permutation procedures of Fig. 2*A*. Our goal was to establish statistically whether oscillations in the original trace that are visible by inspection were not ones expected by chance as might happen in some of the surrogate traces. *C*: power spectrum of the trace in *A* during the interval following the initial microsaccadic suppression period of 100 ms. Colored pixels indicate times and frequency bands with a significant oscillation that is not expected by chance from the surrogate traces (Fig. 2; see MATERIALS AND METHODS).

shows the number of trials within each time bin used to obtain the data in Fig. 3*A*, *top*. In Fig. 3*A*, *bottom*, the time course of number of trials was analyzed using the same running window as that used in Fig. 3*A*, *top*. As can be seen from Fig. 3*A*, *top*, for up to ~100 ms, RT was increased relative to the mean, and it gradually decreased back to "baseline," consistent with a short-lived "microsaccadic suppression" effect known to influence both RT and visual sensitivity in SC and other brain structures (Chen and Hafed 2017; Chen et al. 2015; Hafed and Krauzlis 2010). Interestingly, after ~100 ms, the RT recovery was not back toward a "stable" baseline. Instead, RT kept fluctuating in a rhythmic fashion, becoming sequentially either faster or slower than average (e.g., see the period labeled "Oscillation" in Fig. 3*A*). Moreover, this oscillation was long-lasting and persisted for almost the entire 800 ms that we sampled, and it also occurred when we only included trials with microsaccades less than a 30-min arc in amplitude (Fig. 3*A*, thin green curve). The oscillation was also present (Fig. 3*A*, *inset*) when we first averaged all trials of a single subject into a single curve and then averaged all the individual subjects' single traces to obtain a grand average, as is often done in other studies (e.g., Fiebelkorn et al. 2013).

Since microsaccades have an intrinsic rhythm to them (Bosman et al. 2009; Hafed and Ignashchenkova 2013; Tian et al. 2016), we excluded the possibility that the fluctuations in Fig. 3*A* reflected the occurrence of subsequent microsaccades coming in a rhythmic fashion. Specifically, in our analyses, there was only one single microsaccade before target onset in the analyzed intervals, by design, even for stimuli appearing >700 ms after a movement. To confirm this, we inspected eye velocity traces from all of our accepted trials and ensured that there were no spikes in velocity after the spike associated with the microsaccade of interest. For example, the black radial eye velocity trace of Fig. 4*A* shows average eye velocity from all accepted trials, with only a peak at the microsaccade of interest. In contrast, when we plotted average eye velocity after a randomly chosen microsaccade irrespective of whether a subsequent microsaccade had occurred or not, we obtained the dashed gray curve in Fig. 4*A*. As expected, this curve was elevated compared with the black one, with a peak occurring

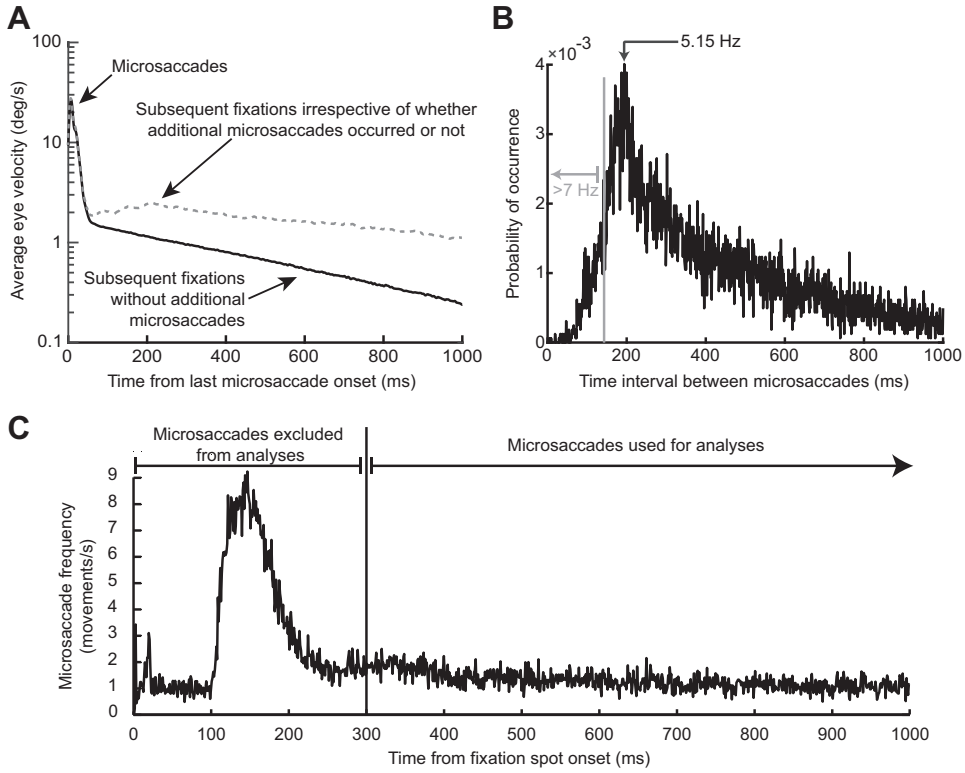

Fig. 4. The RT oscillation in Fig. 3 was not due to either intrinsic microsaccadic rhythms or visual transients associated with the onset of the fixation spot at trial beginning. *A*: the black curve shows mean eye velocity after the last detected microsaccade before target onset from all trials in Fig. 3. For comparison, the dashed gray curve shows mean eye velocity after any given microsaccade irrespective of whether there were subsequent microsaccades or not (from a similar number of trials). The black curve is characterized by an absence of positive-going fluctuations in eye velocity after the first microsaccade (at 0 ms), whereas the gray curve shows elevations peaking at ~200 ms and persisting later, consistent with the likelihood of observing subsequent microsaccades (also see *B*). A similar result was also obtained for *experiment 2*. *B*: distribution of intermicrosaccadic intervals in *experiment 1*. If 2 microsaccades occurred before target onset, the time between the final microsaccade and target onset contributed to our analyses (Fig. 1*A*), but the time between the two microsaccades allowed us to estimate intrinsic microsaccadic rhythms. As can be seen from the histogram, intrinsic microsaccadic rhythms might predict dominant oscillations of ~5 Hz or less, which is lower than any of the oscillations that we observed in our data (> 7 Hz; also see Fig. 5). *C*: microsaccade rate after fixation spot onset. In the interval >300 ms after fixation spot onset, microsaccade rate was constant. We chose to analyze only trials in which the last microsaccade before target onset occurred >300 ms after the beginning of any given trial, to make sure that the effects presented in this study were not phase locked to fixation spot onset. Similar results were obtained from *experiment 2*.

near ~200 ms, reflecting normal intermicrosaccadic intervals and a subsequent plateau reflecting the elevated likelihood of obtaining microsaccades throughout the remaining time interval. Consistent with this, intermicrosaccadic intervals in our data (Fig. 4*B*) peaked at ~200 ms and had a broad tail later. This means that the oscillations in Fig. 3*A* were not due to the occurrence of subsequent microsaccades. This was further confirmed when we considered the details of the intermicrosaccadic interval distribution shown in Fig. 4*B* more closely. According to this distribution, an oscillation dictated by when subsequent microsaccades are triggered would necessarily need to be ~5 Hz (the inverse of ~200 ms) or lower in frequency. However, and as we show in more detail next, our oscillations were significantly higher in frequency, where there would be no microsaccades (see region >7 Hz in Fig. 4*B*). Thus microsaccades have a persistent influence on RT modulations, revealing a coherent long lasting oscillation.

We analyzed the spectral properties of the RT oscillation by computing time-frequency plots in the range of 2–20 Hz. Critically, we performed data shuffling to investigate whether oscillatory rhythms in any given frequency band were expected by chance. Such data shuffling (described in detail in MATERIALS AND METHODS as well as in Fig. 2) gave us a set of surrogate traces, examples of which are shown in Fig. 3*B*, and our goal was to ask whether our original data (Fig. 3, *A* and *B*, *top*) was significantly different from these surrogate traces. In Fig. 3*C*, we only plotted time points after 100 ms (i.e., after the initial microsaccadic suppression interval), and we also only labeled time/frequency ranges that were statistically significant according to conservative criteria (Fig. 2 and see MATERIALS AND METHODS). RT oscillated in the α- and β-frequencies (i.e., within ~8–20 Hz) (Wang 2010); the oscillation gradually decreased in frequency, starting in the low-β/high-α range (i.e., ~10–20 Hz) and then finishing in the low-α range (i.e., ~8–10 Hz).

We also considered the possibility that the RT oscillation was not due to microsaccades but instead to the visual transient associated with fixation spot onset at trial beginning, which could globally reset the visual system. If microsaccades were temporally synchronized to such onset, then the RT oscillation could in reality reflect phase locking to the visual event and not to microsaccades. However, we only analyzed trials with >300 ms of steady fixation. This ensured that we excluded any microsaccades synchronized with fixation spot onset. Indeed, we did find that the likelihood of microsaccades was elevated in the first 300 ms after fixation spot onset (Fig. 4*C*), so

removing these trials was necessary to avoid possible ambiguities about whether phase locking was to the fixation spot onset or not. We also plotted RT time courses as a function of time of target onset from fixation spot onset and irrespective of microsaccades. We found no oscillation but instead a strong RT cost in the first ~500 ms followed by a return to baseline (data not shown); such early RT cost is to be expected given the increased microsaccade likelihood in this early period, since microsaccadic suppression is associated with RT increases.

We also performed DFT analysis on the RT time course of Fig. 3*A* in the period between 100 and 400 ms after microsaccade onset. We found significant power ($P < 0.05$; see MATERIALS AND METHODS) in the range of ~10–16 Hz consistent with Fig. 3*C*. Such significant power also existed when performing the DFT analysis for only trials with microsaccades less than the median amplitude (14.6-min arc) but not for microsaccades larger than the median amplitude (although a nonsignificant peak in a similar frequency range was still evident).

To summarize, our results so far suggest that microsaccades influence RT in a rhythmic fashion for several hundreds of milliseconds (Fig. 3), that this effect also holds for the smallest movement amplitudes, and that this effect cannot be explained by either microsaccade frequency or by visual transients associated with trial onsets (Fig. 4).

Sequential Hemifield Pulses of α- and β-Frequency RT Oscillations After Microsaccades

Even if visual transients associated with trial onsets were not responsible for our results, it could still be the case that the RT oscillation was due to visual transients associated with microsaccades themselves, since microsaccades shift and refresh retinal images. Additionally, a putative extra-retinal influence associated with movement triggering might contribute. In this case, microsaccade direction might have differential effects, since microsaccade generation would necessarily cause lateralized activation of the oculomotor system (Hafed 2011; Hafed et al. 2009, 2015; Hafed et al. 2009; Hafed and Krauzlis 2012; Krauzlis et al. 2017). We thus separated microsaccades according to the visual hemifield to which they were directed. For example, if a microsaccade was directed to the right hemifield, we asked how RT was modulated for rightward targets (presented in the "same hemifield" as the microsaccade) as opposed to leftward ("opposite") ones. Immediately after a microsaccade (and for up to ~100 ms), both "same" and "opposite" targets experienced increased RT as expected from microsaccadic suppression (Fig. 5, *A* and *D*). However, surprisingly, separating movement directions revealed that the coherent oscillation in Fig. 3 consisted of two separate oscillating "pulses" appearing sequentially in each hemifield, and these observations persisted even when considering only microsaccades less than a 30-min arc in amplitude (green traces in Fig. 5, *A* and *D*). From ~160 to 360 ms, a low-β/high-α-oscillation pulse appeared in the same hemifield as the microsaccade (Fig. 5*A*); for target onsets ~380–635 ms after microsaccades, a lower α-pulse appeared in the opposite hemifield (Fig. 5*D*). We obtained these specific frequency ranges by repeating the analyses highlighted in Fig. 2 for the present data subsets to assess statistical significance in the spectrotemporal domain. Specifically, we obtained surrogate traces, examples of which

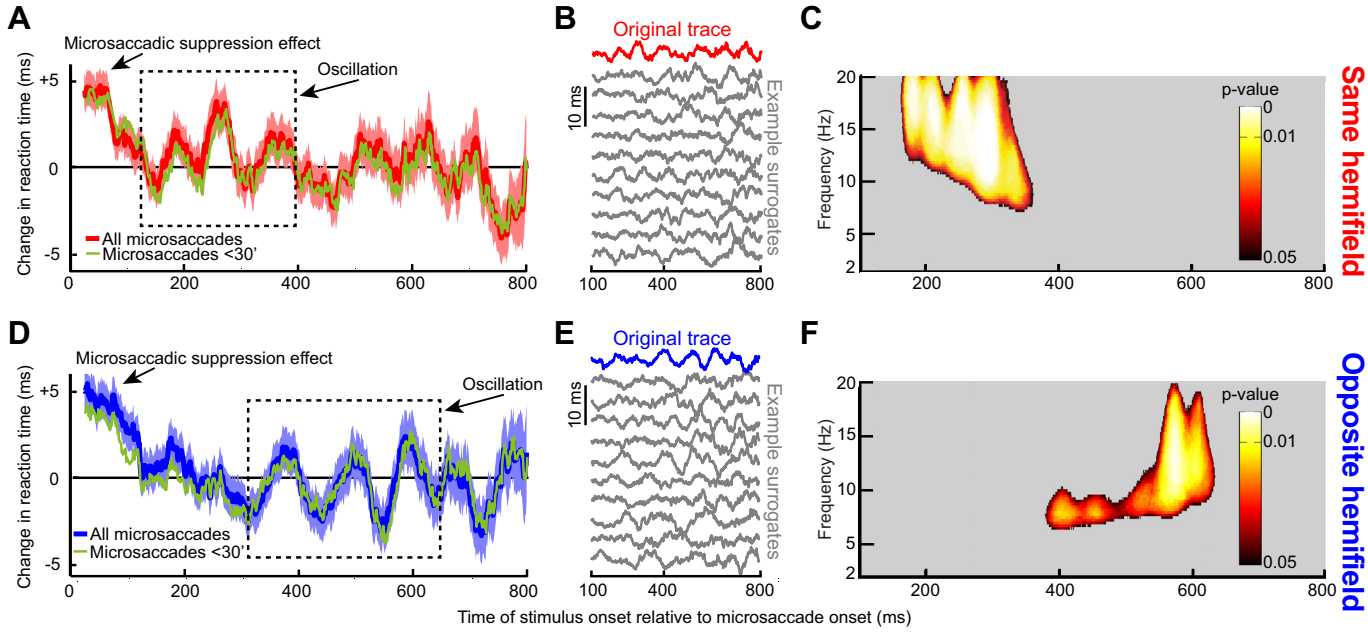

Fig. 5. Dependence of RT oscillations on microsaccade direction. *A*: same analysis as in Fig. 3*A* but only for trials with the target appearing in the same hemifield as a microsaccade. There was an initial microsaccadic suppression effect, followed by an oscillation. However, the oscillation only lasted for up to ~400 ms as indicated by the dashed rectangle, which highlights a pulse of statistically significant RT oscillation (see *C*). *B*: original and example surrogate traces from the data in *A*, as in Fig. 3*B*. *C*: same analysis as in Fig. 3*C* illustrating that the statistically significant RT oscillation pulse was restricted to only the first part of our sampled period after microsaccades. *D*–*F*: same as *A*–*C* but for targets appearing in the opposite hemifield. In this case, the RT oscillation pulse was delayed relative to *A*–*C* (dashed rectangle in *D*; also see *F* for the statistically significant times and frequencies). Thus, when separating microsaccade directions, we found that the long-term RT oscillation in Fig. 3 reflected sequential hemifield gating of RT oscillatory pulses first in the same hemifield as a microsaccade and then in the opposite hemifield. Moreover, the effect was consistent across individual subjects (Fig. 6). Green traces show the RT time courses for microsaccades less than a 30-min arc in amplitude.

are shown in Fig. 5, *B* and *E*, and we then computed significant time-frequency clusters shown in Fig. 5, *C* and *F*). These clusters confirm the sequential nature of the oscillations across hemifield that were evident in Fig. 5, *A* and *D*.

We next assessed the consistency of same- and opposite-hemifield RT oscillation pulses across individual subjects. In Fig. 6*A*, we plotted the phase of 13- to 20-Hz oscillations for an RT curve like that shown in Fig. 5*A* but now obtained from each subject individually. We found that the phase was largely consistent across subjects during the initial same-hemifield RT pulse of Fig. 5*A*, and it got scrambled later (Fig. 6*A*). This was further supported by plotting the PLV (see MATERIALS AND METHODS) of the phase traces shown in Fig. 6*A* (Fig. 6*B*). The shaded gray region in this case (Fig. 6*B*) indicates the time interval during which the PLV was statistically significant according to permutation tests with 1,000 surrogate analyses ($P < 0.05$; see MATERIALS AND METHODS). In other words, during the early same-hemifield RT pulse shown in Fig. 5, *A* and *C*, PLV in our real data from individual subjects consistently deviated from chance expectations obtained from the surrogate traces. We also performed similar analyses for the opposite-hemifield trials, this time within a frequency band (8–12 Hz) consistent with the opposite-hemifield pulse frequency range in Fig. 5, *D* and *F*. Once again, phase was consistent across individuals, but only in the late period in which the opposite-hemifield RT oscillation pulse occurred in Fig. 5, *D* and *F* (Fig. 6, *C* and *D*). Thus the opposite-hemifield RT oscillation pulse in Fig. 5, *D* and *F*, was consistently observed across individual subjects. These results, combined, reveal that microsaccade-phase-locked RT oscillations are dependent on movement direction.

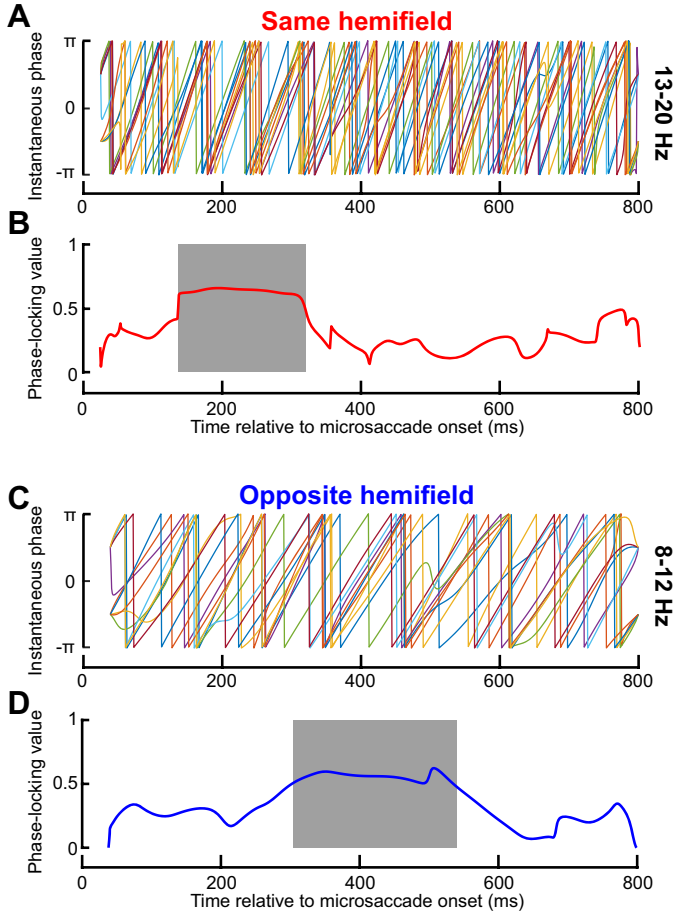

Fig. 6. Consistency of same- and opposite-hemifield RT oscillation pulses across individual subjects. *A*: phase of 13- to 20-Hz oscillations for each subject. Phase was largely consistent across subjects during the initial same-hemifield RT pulse of Fig. 5*A*, C, but it was inconsistent later. *B*: phase-locking value (PLV; see MATERIALS AND METHODS) of the phase traces shown in *A*. The shaded region shows the interval with significant PLV ($P < 0.05$; see MATERIALS AND METHODS), which was consistent with the early pulse in Fig. 5, *A* and *C*. Thus the results in Fig. 5, *A* and *C*, were reliable across individual subjects. *C*: similar analyses but for opposite hemifield trials. Once again, phase was consistent across individuals but only in the late period in which the opposite-hemifield RT oscillation pulse occurred in Fig. 5, *D* and *F*; also see *D*. Thus the opposite-hemifield RT oscillation pulse in Fig. 5, *D* and *F*, was consistently observed across individual subjects. *D*: same as in *B* but for the data in *C*.

Same-Hemifield Advantage in Perceptual Detection During the First α- and β-frequency Oscillatory RT Pulse

In *experiment 2* (Fig. 1*B*), we asked whether visual detection capabilities can also be affected long after microsaccades. We performed this experiment on 14 subjects who had to detect a small, briefly flashed target (see MATERIALS AND METHODS). Target contrast was continuously adjusted to maintain an average correct detection performance of ~50%. This means that subjects reported consciously seeing the target, and correctly localized it, on ~50% of the trials (see MATERIALS AND METHODS). Because this meant that the task was difficult, we placed visual placeholders to aid subjects in estimating the two possible target locations (Fig. 1*B*).

In Fig. 7*A*, *top*, we plotted the proportion of correct target detections as a function of time after microsaccades. Immediately after microsaccade onset, and for ~100 ms, subjects had immense difficulty in seeing the target; their likelihood of reporting that they saw the target and with correct localization was lower than the ~50% goal of this experiment's design (this means that they pressed "target not seen" more often than they pressed a seen target location). This is consistent with microsaccadic suppression. Interestingly, after such suppression, and specifically during the period in which the same-hemifield RT oscillation pulse occurred in Fig. 5, *A* and *C*, perceptual detection in the present experiment was also higher for the target appearing in the same vs. opposite hemifield as the microsaccade (dashed rectangle in Fig. 7*A*, *top*; $P = 0.0033$ in the interval 100–400 ms; 2-proportion *z*-test; also see Fig. 7*C*). This effect is remarkable because it emerged even though task difficulty was continuously titrated to maintain ~50% performance. This effect is also reminiscent of other observations made on shorter analysis time intervals than ours (Yuval-Greenberg et al. 2014), although it is not clear whether these authors analyzed performance during microsaccadic suppression or after it (Tian and Chen 2015). For later times, performance in both hemifields was similar (Fig. 7*A*, *top*; $P = 0.8035$ in the interval 400–800 ms; 2-proportion *z*-test). These results suggest that during the first RT oscillation pulse in the same hemifield observed in Fig. 5, perceptual detection capabilities were also improved (Fig. 7*A*). However, we did not find any statistically significant high-frequency oscillations in performance as we did for RT.

The early same-hemifield perceptual detection improvement (Fig. 7*A*) was also consistent across individuals (Fig. 8*A*), further suggesting that this effect was a robust property of

long-term microsaccadic influences. However, we have to emphasize here that we were unable to realize statistical significance on a per-subject basis due to the low numbers of trials per subject; nonetheless, all but three subjects showed trends consistent with our pooled observations (Fig. 8*A*).

We also ensured faithful task performance by the subjects despite task difficulty. For example, incorrect reports of target location were much less frequent than correct responses (Fig. 7*A*, *bottom*), and only 8% of catch trials had false alarms. This means that subjects followed the instruction to only report targets when they were consciously seen. Similarly, we ensured that target contrast was not different between same and opposite trials when performance was different. Specifically, in Fig. 8*B*, we compared target luminance contrast between the two sets of trials and confirmed that target contrast could not explain the early same-hemifield performance advantage observed in Fig. 7*A*.

It could also be suggested that the improved perceptual performance in Fig. 7*A* (dashed rectangle) was due to microsaccades bringing the fovea slightly closer to the peripheral target than with oppositely directed movements. Indeed, when we measured the position of the peripheral target relative to the fovea at the time of target onset in trials with improved perceptual performance (i.e., with targets 100–400 ms after microsaccades), we found that the target was slightly closer to the fovea on same than opposite trials (Fig. 7*B*, *left*), which was due to the eye becoming better aligned to the fixation spot (see Fig. 9). To ask whether this slight difference in retinotopic position was sufficient to explain the same-hemifield advantage, we performed two additional analyses. First, we only took trials in which target position overlapped between same and opposite trials (see MATERIALS AND METHODS), and we compared detection performance. The same-hemifield advantage was still present ($P = 0.034$ permutation test; see MATERIALS AND METHODS). Second, we reanalyzed the original data by now classifying trials according to the position of the target relative to the fovea rather than according to microsaccade direction (Fig. 7*B*, *right*); we performed a median split on Euclidean distance between target and fovea, and we compared "close" vs. "far" target positions, regardless of microsaccade direction. We no longer observed a difference in performance (Fig. 7*C*), suggesting that our results could not be explained by the target being closer to the fovea on same vs. opposite microsaccade trials. Consistent with this, we still observed the same-hemifield advantage when restricting our analyses to only trials with microsaccades less than a 30-min arc in amplitude and even those with microsaccades less than the median amplitude of a

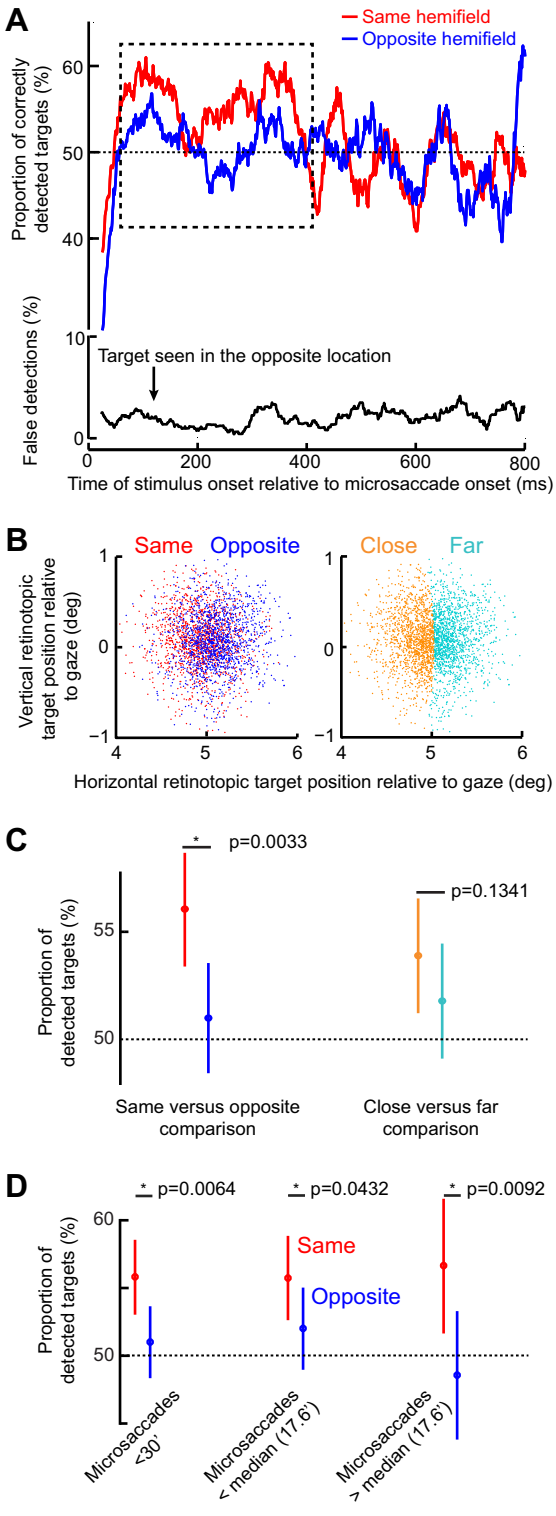

Fig. 7. Same-hemifield advantage in detectability during the period of the initial RT pulse. *A*, *top*: mean detectability (i.e., correct responses) as a function of time after microsaccade onset. Immediately after microsaccades, detectability was impaired, consistent with microsaccadic suppression effects (see MATERIALS AND METHODS). However, in the dashed rectangle, which corresponds closely with the same-hemifield RT pulse in Fig. 5, *A* and *C*, detectability was significantly higher for targets appearing in the same hemifield as a microsaccade than for opposite targets ($P = 0.0033$; 2-proportion *z*-test). *A*, *bottom*: incorrect target localizations, which were rare and unmodulated by microsaccadic suppression, suggesting that subjects followed task instructions (also see RESULTS). *B*: retinotopic target position at the time of target onset for trials in the early (100–400 ms) interval after microsaccade onset (each dot is a trial). Positions are colored based on the direction of the last microsaccade relative to the target (*left*) or whether the target was closer or farther than the median Euclidean distance observed. *C*: mean detectability during the early (100–400 ms) period. The *left pair* compares conditions when the target was presented in the same or opposite hemifield relative to a microsaccade. The *right pair* compares closer or farther targets from the fovea. Detectability was only enhanced in the same hemifield condition (*left*) and did not depend on retinotopic target position (*right*). *D*: mean detectability as in *C* but now only when microsaccades were less than a 30-min arc in amplitude or when they were smaller or bigger than the median. In all cases, the same-hemifield advantage of *A* was observed. Error bars denote 95% confidence intervals.

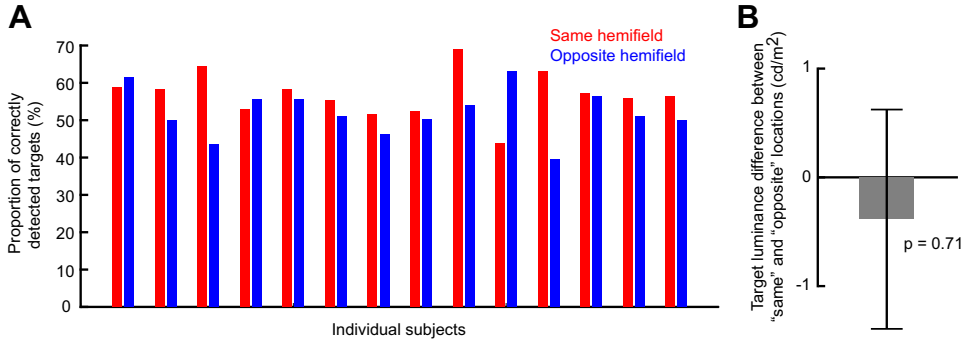

Fig. 8. Individual subject data and same vs. opposite target contrasts in *experiment 2*. *A*: mean detectability for each subject and each target hemifield location relative to microsaccade direction in the perceptual detection task. This analysis is restricted to the early period (100–400 ms) after microsaccade onset, which is the period in which we observed differential detection performance across hemifields (Fig. 7). Note that 11 out of the 14 subjects detected the target better when it was presented in the same hemifield as the microsaccade, consistent with the overall population average results in Fig. 7. Thus no outlier subject minority was responsible for the differences observed in Fig. 7 when the data were averaged across all participants. *B*: difference in target contrast between same and opposite trials in the early period. There was no statistically significant difference ($P = 0.71$; *t*-test), suggesting that the performance differences in Fig. 7 were not due to differences in target contrast. Error bar denotes SE.

17.6-min arc (Fig. 7*D*). For these trials, retinotopic target position was very similar between same and opposite trials.

Finally, we wondered whether our results could reflect microsaccades being pulled peripherally by a rhythmic process of covert peripheral visual attention, as suggested by recent evidence (Busch et al. 2009; Busch and VanRullen 2010; Dugué et al. 2015; Fiebelkorn et al. 2013; Landau and Fries 2012; Landau et al. 2015; Song et al. 2014). We analyzed microsaccade directions relative to the fixation spot (Fig. 9) and confirmed previous findings that microsaccades redirect gaze to the spot and not the periphery (Buonocore et al. 2017; Guerrasio et al. 2010; Ko et al. 2010; Tian et al. 2016). That is, eye position was closer to the fixation spot after microsaccades than before them (Fig. 9). Thus our results are likely due to microsaccade generation itself. Of course, some relation to peripheral covert attention might still be expected (Hafed 2013; Tian et al. 2016) given our results, as we discuss in more detail in DISCUSSION.

Postsuppression Enhancement in SC Visual Sensitivity After Microsaccades

Finally, because our *experiment 1* was motivated by our recent SC studies relating perimicrosaccadic visual sensitivity in this brain structure to RT (Chen and Hafed 2017; Hafed and Krauzlis 2010), we revisited these studies from the perspective of what we have learned so far from the present results. We specifically hypothesized that RT oscillations should correlate with visual sensitivity even in the absence of any overt response. In our previous SC studies, visual response strength was the only assay of microsaccadic suppression, and monkeys did not perform any task other than fixation (Chen and Hafed 2017; Hafed and Krauzlis 2010). SC visual response strength in these studies correlated remarkably well with RT effects obtained from completely different behavioral sessions (Chen and Hafed 2017). This means that if we were to record SC visual responses in the absence of any behavioral task, then a faster RT following the initial microsaccadic suppression effect (e.g., Fig. 3) should be mirrored by stronger visual responses than "baseline" (with "baseline" defined as response strength in the absence of any nearby microsaccades; see MATERIALS AND METHODS). We thus analyzed visual response strength after microsaccades in two monkeys, using data from Chen et al. (2015), by extending the time course of analysis beyond the initial 100 ms that we typically used in our earlier studies. For up to ~100 ms after microsaccade onset, visual response strength in both visual and visual-motor SC neurons was suppressed, as expected (Fig. 10). Specifically, the curves in Fig. 10 were below the normalized "baseline" response value of 1 for all time points less than that indicated by the dashed vertical line (error bars denote 95% confidence intervals).

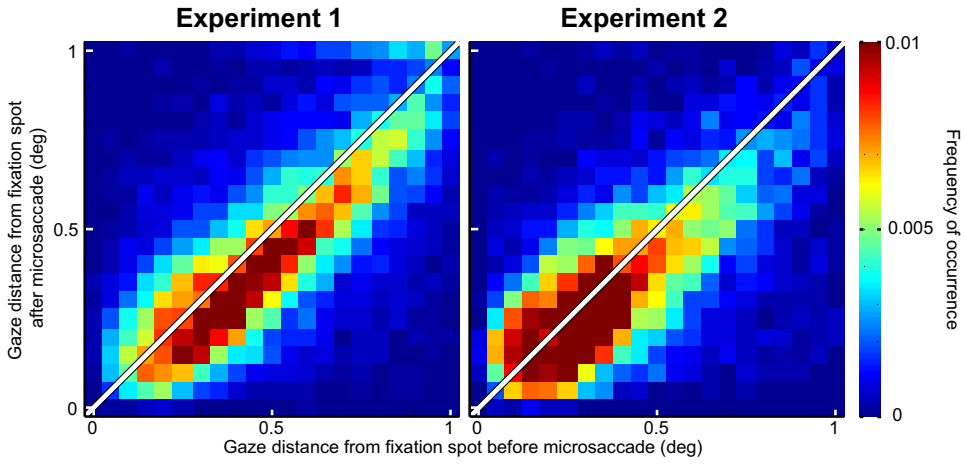

Fig. 9. Microsaccades acted to primarily correct for foveal motor errors during gaze fixation. We plotted gaze distance from the fixation spot before and after microsaccades, for all microsaccades that were used in the analyses of Figs. 3, 5, and 7. During both experiments, microsaccades brought gaze closer to the fixation spot than before the movements ($P = 1.2111 \times 10^{-54}$ in *experiment 1* and $P = 6.9096 \times 10^{-29}$ in *experiment 2*; Wilcoxon rank sum test), consistent with recent observations in previous studies. This suggests that our microsaccades were not necessarily reflecting endogenous attention shifts towards the periphery but were instead part of a deliberate oculomotor strategy to optimize eye position on the fixated target.

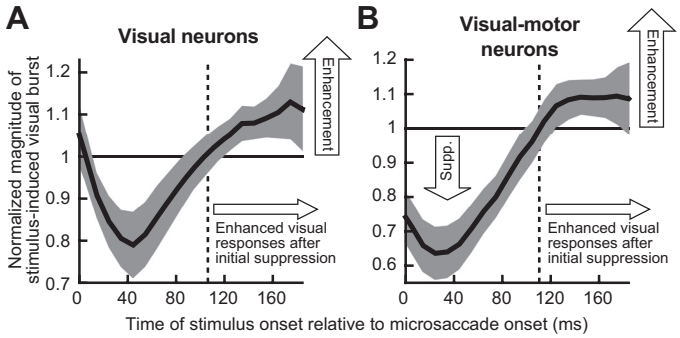

Fig. 10. Neural implications of an RT oscillation after initial microsaccadic suppression. *A*: we performed time course analyses of visual response strength in superior colliculus (SC) purely visual neurons. The neurons were the same as those used in Chen et al. (2015), and the analysis was identical to that performed in Hafed and Krauzlis (2010), except that we extended the analysis window beyond the typical 100 ms after microsaccade onset that we had used earlier (see MATERIALS AND METHODS). This allowed us to explore whether recovery from neural microsaccadic suppression is towards a constant baseline or not, as we did in the behavioral experiment of Fig. 1. Error bars denote 95% confidence intervals. As can be seen, after the initial ~100 ms of neural suppression, visual response strength was enhanced (i.e., the curve went above 1), rather than being equal to "baseline," suggesting that RT oscillations like in Fig. 3 can reflect oscillations in visual neural sensitivity. *B*: a similar observation was made for visual sensitivity of visual-motor SC neurons, which are better correlated to RT (Chen and Hafed 2017; Hafed and Krauzlis 2010). In *A* and *B*, the "baseline" response (normalized to 1) was obtained from trials in which there were no microsaccades within ±150 ms from stimulus onset. Note that this data set did not allow us to sample neural sensitivity for longer periods after a microsaccade (as in Fig. 3), but the postsuppression enhancement nonetheless suggests that visual neural fluctuations can also go above baseline, consistent with the Fig. 3 RT oscillation.

Interestingly, visual response strength in both visual and visual-motor SC neurons indeed increased above baseline after this initial microsaccadic suppression (Fig. 10; curves lying above 1 in the interval after the vertical dashed line). Thus, like RT costs, recovery from neural microsaccadic suppression was also not back to a single "baseline," but there was higher visual sensitivity after the initial suppression. These neural analyses did not allow us to extend the time course for hundreds of milliseconds like in our behavioral data, because our earlier neural experiments did not sample long times after microsaccades (Chen et al. 2015); however, they nonetheless demonstrate that our RT effects in Fig. 3 may be related to visual sensitivity modulations after microsaccades, as suggested earlier (Chen and Hafed 2017; Hafed et al. 2015; Hafed and Krauzlis 2010; Tian et al. 2016). This is also similar to behavioral results with large saccades showing enhancement after the suppression (Burr et al. 1994; Diamond et al. 2000; Knöll et al. 2011). We also saw hints of direction dependence in the post-suppression enhancement of neural activity in Fig. 10, similar to Fig. 5, but the data (constrained by prior neural recordings) were not sufficient to allow us to establish statistical significance.

DISCUSSION

We found that microsaccade occurrence has a profound long-term influence on brain state, resulting in coherent pulsed α/β-RT oscillations first in the same visual hemifield as the movement vector and then in the opposite hemifield. We also found long-term changes in perceptual detection and SC neural activity. In what follows, we discuss these observations and relate them to observations of physiological rhythms in the brain, attentional fluctuations, and motor control in general. We also discuss our methodological choices and their potential limitations.

We think that the lateralization of the two oscillatory pulses that we observed in RT (Fig. 5) is likely jumpstarted by microsaccade movement commands, which necessarily result in lateralized action-potential bursts in spatially organized visual-motor structures like the SC (Hafed et al. 2009; Hafed and Krauzlis 2012). Interestingly, the switch to the opposite hemifield RT oscillation that we observed in Fig. 5, *D–F*, came at approximately the time at which one would normally make a second eye movement during natural scene viewing and also during fixation in the case of microsaccades (e.g., Fig. 4*B*). It would be interesting to investigate the implications of such hemifield switching under more natural conditions. For example, there is evidence for "facilitation of return" in saccadic scanning of natural scenes (Wilming et al. 2013), in which "return saccades" are frequently observed (i.e., a saccade occurs opposite in direction to a previous one). It might be the case that the brain mechanisms underlying the sequential hemifield switches that we have observed could be related to such increases in the propensity to make return saccades. This can also apply in the case of scanning objects in far environments, in which microsaccades would be necessary given the small images projected by far visual features onto the retina. Thus the results that we obtained in a laboratory setting with a fixation marker can potentially be extended to more naturalistic scenarios.

We also think that our results may be related to observations of neural oscillatory patterns in a variety of visual areas. For example, it was previously shown that microsaccades cause broadband modulation of visual areas immediately after movements (Bosman et al. 2009; Lowet et al. 2016). This is consistent with image refreshing (Martinez-Conde et al. 2000), but there could also be longer term oscillations in neural activity, and future work should explore the links between neural and behavioral oscillations in relation to microsaccades. Currently, such links may not always be obvious, especially because during parts of the longer term intervals that we have focused on here, some visual areas were shown previously to exhibit low frequency oscillations and not higher frequency ones like we saw. For example, the neural oscillations that were reported previously were primarily consistent with microsaccade frequency (Bosman et al. 2009) and not necessarily with the higher frequencies that we observed in our data. Similarly, if neural oscillation results were indeed to turn out to be linked to our behavioral observations, then we think that longer term analyses of neural data (say, at 600 ms or more after a movement) need to take microsaccade direction into account. For example, the neurophysiological experiments of Bosman et al. (2009) did not separate different movement directions, and this could be why oscillatory patterns may not have lasted for too long (if there is sequential hemifield pulsing but all movements are combined, then such pulsing might be masked). Indeed, even at the neural level, movement direction does seem to matter a great deal for large saccades, which are associated with direction-dependent β-frequency waves in area V4 (Zanos et al. 2015). α-Oscillations have also been observed in V4 after large saccades (Zanos et al. 2016), but these

oscillations were once again short-lived because potential later oscillations in the opposite hemifield were not investigated.

Related to the above, we observed α- and β-behavioral oscillations in RT (Figs. 3 and 5). The β-oscillations that we observed might be a lingering component of β-rhythms associated with microsaccade generation, since β-rhythms can be movement-related (Wang 2010). On the other hand, the α-oscillations may be related to occipital α-rhythms, which synchronize to microsaccades (Gaarder et al. 1966). Of course, this requires an assumption that occipital modulations can manifest in RT modulations, but this is quite reasonable. In fact, even manual RT is a highly sensitive measure of properties of the early visual system, like magno- and parvo-cellular pathways (Breitmeyer 1975). Similarly, the early evoked visual response of SC neurons is highly predictive of RT's collected from separate sessions (Chen and Hafed 2017). In this regard, such sensitivity of RT could be why it was easier to see significant oscillations in *experiment 1* than in *experiment 2*. Indeed, maybe more data would have revealed significant oscillations also in *experiment 2*, but this itself would indicate that the effect is less robust. The visual stimuli were also very different in both experiments, so it could be that our task in *experiment 2* was not sensitive enough to behaviorally manifest the underlying brain oscillations. It is nonetheless still interesting that the same-hemifield advantage in Fig. 7 emerged at the same time as the same-hemifield RT oscillation pulse in Fig. 5.

The above statements suggest that the implications of our findings are not necessarily that RT or detection effects in our present scenarios are the ultimate goal of microsaccade-related synchronization of endogenous brain rhythms. Rather, we think that our behavioral assays were sensitive measures of underlying oscillations, which could be useful in a variety of other ways. For example, oscillations could increase the efficacy of transmitting information between areas (for example, from the lateral geniculate nucleus to primary visual cortex) (Bastos et al. 2014). This could happen, say, through the so-called idea of "communication through coherence" (Fries 2005). Additionally, the phase of oscillations slower than 20 Hz could be used to potentially increase the information conveyed by each spike in V1 (Montemurro et al. 2008), and α-oscillations could order and prioritize salient information from the unattended visual field (Jensen et al. 2012). In this regard, such oscillations could modulate when and how neural assemblies might inhibit other assemblies. Overall, this could help in allocating resources to "sample" different regions of an image. At the circuit level, oscillations can also emerge out of known microcircuit architecture in cortex with local inhibitory loops, so they also represent structure-function relationships in brain operation.

In our experiments, we also observed higher oscillation frequencies than those predicted by attentional sampling at the behavioral level (Fiebelkorn et al. 2013; Landau and Fries 2012). However, our results are still consistent with hypotheses about perceptual rhythms in the visual system (Busch et al. 2009; Busch and VanRullen 2010; VanRullen 2016), and we think that it is quite reasonable that these rhythms would be related to saccades and microsaccades, especially given how active visual perception is under natural conditions.

With respect to attention, it could additionally be argued that covert attention might have been the source of the RT oscillations and same-hemifield detection advantages that we have observed, independently of microsaccades. Indeed, attention samples locations rhythmically (Busch et al. 2009; Busch and VanRullen 2010; Dugué et al. 2015; Fiebelkorn et al. 2013; Landau and Fries 2012; Landau et al. 2015; Song et al. 2014), and microsaccades are correlated with attention (Engbert and Kliegl 2003; Hafed and Clark 2002; Hafed et al. 2011). However, time locking of our effects to microsaccades would require that the time and direction of any given movement would have to perfectly match the time and direction of every single attention shift or at least within a small window associated with β-rhythms (<50 ms). Moreover, we found that microsaccades correct for eye position error (Fig. 9), consistent with previous findings (Guerrasio et al. 2010; Ko et al. 2010; Tian et al. 2016), rather than increase such error, which is what would happen if they were pulled peripherally by oscillations in the locus of peripheral covert attention. Instead, we think that our results are more likely related to well-known perimicrosaccadic influences on visual sensitivity, as in the case of microsaccadic (Chen et al. 2015; Hafed et al. 2015; Hafed and Krauzlis 2010; Zuber and Stark 1966) and saccadic (Benedetto and Morrone 2017) suppression. However, even with this view, a relation to attention can still be expected (Hafed 2013; Hafed et al. 2015; Tian et al. 2016). For example, since microsaccades are reflexively reset by sensory cues (Hafed and Ignashchenkova 2013; Rolfs et al. 2008), it may be possible based on our current results that some behavioral effects in attention tasks may be partially influenced by microsaccades occurring several hundreds of milliseconds before a target.

It was also recently found that large voluntary saccades are associated with behavioral performance oscillations like in our results (Benedetto and Morrone 2017; Hogendoorn 2016; Wutz et al. 2016). However, an intriguing difference between these observations and ours is that our oscillations were higher in frequency than in these studies. Indeed, the lower frequency oscillations associated with large voluntary saccades may be related either to attentional rhythms (Hogendoorn 2016) or the intrinsic saccadic/microsaccadic rhythms of the oculomotor system (Benedetto and Morrone 2017), which are both slower than the α- and β-frequencies that we observed. Since microsaccades cannot be generally made at such high frequencies (e.g., Fig. 4*B*), this leads us to hypothesize that microsaccades may "ride" on slow frequency rhythms, as we have recently suggested (Tian et al. 2016), and as is the case with the large saccade results of Benedetto and Morrone (2017) and Hogendoorn (2016), but that they reset the phase of higher frequency oscillations. Such resetting could serve the purpose of regularizing visual processing in between two successive movements (Chen and Hafed 2017), particularly with the sequential hemifield pulsing that we observed. Interestingly, our DFT analysis did not reveal significant ~10- to 16-Hz oscillations for microsaccades larger than the median amplitude, but there was also a secondary peak at ~4–5 Hz (although still non-significant) emerging for these larger microsaccades. It would be interesting to investigate the interactions between multiple frequency bands and saccade/microsaccade sizes at the mechanistic level in future research.

Finally, our observation of coherent effects when pooling multiple subjects' data suggests that our observations were common across individuals, even if there may have been individual differences in more subtle ways (in, say, the exact

values of α- or β-oscillation frequencies that each individual might exhibit). We find both this observation and the fact that the coherent oscillations appeared at the behavioral level (i.e., at the overall output of the entire brain processing cascade) intriguing. In this sense, a small effect size (e.g., for the absolute RT difference between peak and trough in Fig. 3*A*) is to be perfectly expected after pooling all subjects together; what is more interesting is that such a coherent effect occurs at all in the first place. Also, amplitudes of behavioral oscillations at the high frequencies that we studied are generally mild even in earlier studies (Song et al. 2014). Thus it is the phase consistency after pooling that is interesting here, rather than the effect size itself. Having said that, it may still be argued that an across-subject average oscillation can emerge even if individual subjects had no oscillations at all, but if they instead each somehow had a "strategically timed" single peak in RT (to give rise to the highly specific results in Figs. 3 and 5 after pooling). This is both physiologically and statistically unlikely, but we explored it further by running one of our monkeys on multiple sessions of a version of *experiment 1* to obtain reliable within-subject RT time courses. The results that we obtained (Fig. 11), which are part of an ongoing follow-up investigation of neural mechanisms, confirmed that multiple RT peaks can indeed appear within an individual subject.

The above points touch on the importance of statistical analyses in studies like ours. In our approach, we pooled subjects but this was because of the daunting task of data collection (e.g., the number of trials per time bin in Fig. 3*A* was an order of magnitude smaller than the total number of trials collected because of factors related to Fig. 4). However, we were careful to correct for multiple comparisons and other factors in analyses, especially because running average operations can cause ringing in traces that may appear to be an oscillation visually even when there is no oscillation (e.g., see some surrogate traces in Figs. 3*B* and 5, *B* and *E*). We find it unlikely that our results were entirely explained by ringing, especially given the sequential hemifield pulsing that we observed in Fig. 5 (it is not clear how filtering-related ringing artifacts can give rise to such a finding). However, we acknowledge that our filtering choices restricted our analyses to frequencies <20 Hz. It may be possible that higher frequencies are present, but this remains to be seen in future experiments.

Overall, our results bridge action, perception, and rhythmic brain fluctuations in a manner that should helpfully inform many exciting future neurophysiological experiments in vision science.

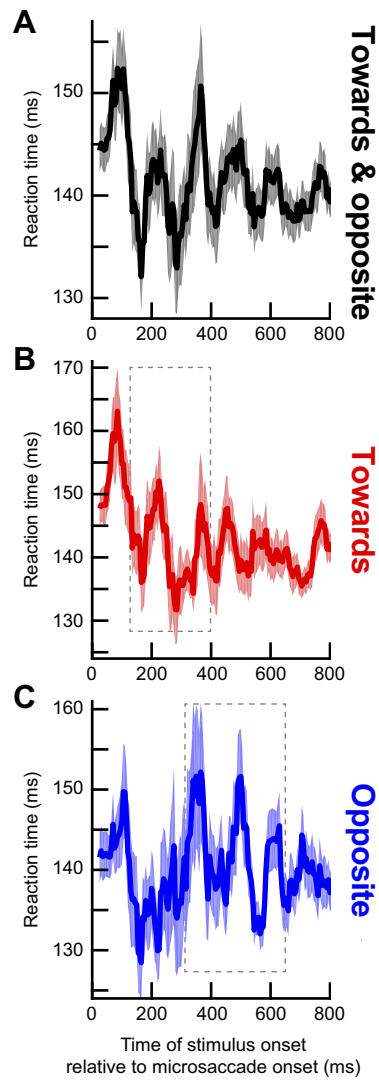

Fig. 11. RT fluctuations within an individual monkey subject. We ran *monkey N* on 11 sessions of a version of *experiment 1*. A target like in *experiment 1* could appear at random times after microsaccades, but it could appear at one of eight different equally spaced directions. We defined microsaccades as being towards or opposite the target if their directions were within ±22.5° from the direction of the target or the direction diametrically opposite it. *A*: an analysis like that in Fig. 3 (with a 50-ms running window in 5-ms steps) revealed RT fluctuations similar to those in Fig. 3, with multiple peaks at different times; thus multiple peaks of RT variability can indeed happen within an individual subject. Discrete Fourier transform analysis on the shown interval revealed a spectral peak at ~7.7 Hz. *B* and *C*: we repeated the analysis for cases in which the target appeared in a direction congruent with microsaccade direction ("Towards") or opposite it ("Opposite"). The highest amplitude RT fluctuations occurred early for "Towards" microsaccades and later for "Opposite" movements, just like in Fig. 5. As a reference, the thin gray rectangles show the time intervals in which our average analyses in humans showed significant oscillatory pulses in similar conditions (Fig. 5). This monkey showed similar patterns to the pooled human data. Error bars denote SE across trials, and the figure is formatted similarly to Figs. 3 and 5.

ACKNOWLEDGMENTS

We are grateful for helpful comments on the manuscript from three peer reviewers.

GRANTS

We were funded by the Werner Reichardt Centre for Integrative Neuroscience (CIN), an Excellence Cluster (EXC307) funded by the Deutsche Forschungsgemeinschaft (DFG). We were also supported by the Hertie Institute for Clinical Brain Research.

DISCLOSURES

No conflicts of interest, financial or otherwise, are declared by the authors.

AUTHOR CONTRIBUTIONS

J.B. and Z.M.H. conceived and designed research; J.B. and Z.M.H. performed experiments; J.B., C.-Y.C., and Z.M.H. analyzed data; J.B. and Z.M.H. interpreted results of experiments; J.B. and Z.M.H. prepared figures; J.B., C.-Y.C., and Z.M.H. edited and revised manuscript; J.B., C.-Y.C., and Z.M.H. approved final version of manuscript; Z.M.H. drafted manuscript.

REFERENCES

Bastos AM, Briggs F, Alitto HJ, Mangun GR, Usrey WM. Simultaneous recordings from the primary visual cortex and lateral geniculate nucleus reveal rhythmic interactions and a cortical source for γ-band oscillations. *J Neurosci* 34: 7639–7644, 2014. doi:10.1523/JNEUROSCI.4216-13.2014.

Benedetto A, Morrone MC. Saccadic suppression is embedded within extended oscillatory modulation of sensitivity. *J Neurosci* 37: 3661–3670, 2017. doi:10.1523/JNEUROSCI.2390-16.2016.

Benedetto A, Spinelli D, Morrone MC. Rhythmic modulation of visual contrast discrimination triggered by action. *Proc Biol Sci* 283: 283, 2016. doi:10.1098/rspb.2016.0692.

Bosman CA, Womelsdorf T, Desimone R, Fries P. A microsaccadic rhythm modulates gamma-band synchronization and behavior. *J Neurosci* 29: 9471–9480, 2009. doi:10.1523/JNEUROSCI.1193-09.2009.

Breitmeyer BG. Simple reaction time as a measure of the temporal response properties of transient and sustained channels. *Vision Res* 15: 1411–1412, 1975. doi:10.1016/0042-6989(75)90200-X.

Buonocore A, Chen CY, Tian X, Idrees S, Muench T, Hafed ZM. Alteration of the microsaccadic velocity-amplitude main sequence relationship after visual transients: implications for models of saccade control. *J Neurophysiol* 117: 1894–1910, 2017. doi:10.1152/jn.00811.2016.

Burr DC, Morrone MC, Ross J. Selective suppression of the magnocellular visual pathway during saccadic eye movements. *Nature* 371: 511–513, 1994. doi:10.1038/371511a0.

Busch NA, Dubois J, VanRullen R. The phase of ongoing EEG oscillations predicts visual perception. *J Neurosci* 29: 7869–7876, 2009. doi:10.1523/JNEUROSCI.0113-09.2009.

Busch NA, VanRullen R. Spontaneous EEG oscillations reveal periodic sampling of visual attention. *Proc Natl Acad Sci USA* 107: 16048–16053, 2010. doi:10.1073/pnas.1004801107.

Chen CY, Hafed ZM. Postmicrosaccadic enhancement of slow eye movements. *J Neurosci* 33: 5375–5386, 2013. doi:10.1523/JNEUROSCI.3703-12.2013.

Chen CY, Hafed ZM. A neural locus for spatial-frequency specific saccadic suppression in visual-motor neurons of the primate superior colliculus. *J Neurophysiol* 117: 1657–1673, 2017. doi:10.1152/jn.00911.2016.

Chen CY, Ignashchenkova A, Thier P, Hafed ZM. Neuronal response gain enhancement prior to microsaccades. *Curr Biol* 25: 2065–2074, 2015. doi:10.1016/j.cub.2015.06.022.

Cherici C, Kuang X, Poletti M, Rucci M. Precision of sustained fixation in trained and untrained observers. *J Vis* 12: 12, 2012. doi:10.1167/12.6.31.

Diamond MR, Ross J, Morrone MC. Extraretinal control of saccadic suppression. *J Neurosci* 20: 3449–3455, 2000.

Dugué L, McLelland D, Lajous M, VanRullen R. Attention searches nonuniformly in space and in time. *Proc Natl Acad Sci USA* 112: 15214–15219, 2015. doi:10.1073/pnas.1511331112.

Engbert R, Kliegl R. Microsaccades uncover the orientation of covert attention. *Vision Res* 43: 1035–1045, 2003. doi:10.1016/S0042-6989(03)00084-1.

Fiebelkorn IC, Saalmann YB, Kastner S. Rhythmic sampling within and between objects despite sustained attention at a cued location. *Curr Biol* 23: 2553–2558, 2013. doi:10.1016/j.cub.2013.10.063.

Fries P. A mechanism for cognitive dynamics: neuronal communication through neuronal coherence. *Trends Cogn Sci* 9: 474–480, 2005. doi:10.1016/j.tics.2005.08.011.

Gaarder K, Koresko R, Kropfl W. The phasic relation of a component of alpha rhythm to fixation saccadic eye movements. *Electroencephalogr Clin Neurophysiol* 21: 544–551, 1966. doi:10.1016/0013-4694(66)90173-8.

Goffart L, Hafed ZM, Krauzlis RJ. Visual fixation as equilibrium: evidence from superior colliculus inactivation. *J Neurosci* 32: 10627–10636, 2012. doi:10.1523/JNEUROSCI.0696-12.2012.

Guerrasio L, Quinet J, Büttner U, Goffart L. Fastigial oculomotor region and the control of foveation during fixation. *J Neurophysiol* 103: 1988–2001, 2010. doi:10.1152/jn.00771.2009.

Hafed ZM. Mechanisms for generating and compensating for the smallest possible saccades. *Eur J Neurosci* 33: 2101–2113, 2011. doi:10.1111/j.1460-9568.2011.07694.x.

Hafed ZM. Alteration of visual perception prior to microsaccades. *Neuron* 77: 775–786, 2013. doi:10.1016/j.neuron.2012.12.014.

Hafed ZM, Chen CY, Tian X. Vision, perception, and attention through the lens of microsaccades: mechanisms and implications. *Front Syst Neurosci* 9: 167, 2015. doi:10.3389/fnsys.2015.00167.

Hafed ZM, Clark JJ. Microsaccades as an overt measure of covert attention shifts. *Vision Res* 42: 2533–2545, 2002. doi:10.1016/S0042-6989(02)00263-8.

Hafed ZM, Goffart L, Krauzlis RJ. A neural mechanism for microsaccade generation in the primate superior colliculus. *Science* 323: 940–943, 2009. doi:10.1126/science.1166112.

Hafed ZM, Ignashchenkova A. On the dissociation between microsaccade rate and direction after peripheral cues: microsaccadic inhibition revisited. *J Neurosci* 33: 16220–16235, 2013. doi:10.1523/JNEUROSCI.2240-13.2013.

Hafed ZM, Krauzlis RJ. Microsaccadic suppression of visual bursts in the primate superior colliculus. *J Neurosci* 30: 9542–9547, 2010. doi:10.1523/JNEUROSCI.1137-10.2010.

Hafed ZM, Krauzlis RJ. Similarity of superior colliculus involvement in microsaccade and saccade generation. *J Neurophysiol* 107: 1904–1916, 2012. doi:10.1152/jn.01125.2011.

Hafed ZM, Lovejoy LP, Krauzlis RJ. Modulation of microsaccades in monkey during a covert visual attention task. *J Neurosci* 31: 15219–15230, 2011. doi:10.1523/JNEUROSCI.3106-11.2011.

Hafed ZM, Lovejoy LP, Krauzlis RJ. Superior colliculus inactivation alters the relationship between covert visual attention and microsaccades. *Eur J Neurosci* 37: 1169–1181, 2013. doi:10.1111/ejn.12127.

Havermann K, Cherici C, Rucci M, Lappe M. Fine-scale plasticity of microscopic saccades. *J Neurosci* 34: 11665–11672, 2014. doi:10.1523/JNEUROSCI.5277-13.2014.

Herrington TM, Masse NY, Hachmeh KJ, Smith JE, Assad JA, Cook EP. The effect of microsaccades on the correlation between neural activity and behavior in middle temporal, ventral intraparietal, and lateral intraparietal areas. *J Neurosci* 29: 5793–5805, 2009. doi:10.1523/JNEUROSCI.4412-08.2009.

Hogendoorn H. Voluntary saccadic eye movements ride the attentional rhythm. *J Cogn Neurosci* 28: 1625–1635, 2016. doi:10.1162/jocn_a_00986.

Jensen O, Bonnefond M, VanRullen R. An oscillatory mechanism for prioritizing salient unattended stimuli. *Trends Cogn Sci* 16: 200–206, 2012. doi:10.1016/j.tics.2012.03.002.

Kliegl R, Rolfs M, Laubrock J, Engbert R. Microsaccadic modulation of response times in spatial attention tasks. *Psychol Res* 73: 136–146, 2009. doi:10.1007/s00426-008-0202-2.

Knöll J, Binda P, Morrone MC, Bremmer F. Spatiotemporal profile of peri-saccadic contrast sensitivity. *J Vis* 11: 15, 2011. doi:10.1167/11.14.15.

Ko HK, Poletti M, Rucci M. Microsaccades precisely relocate gaze in a high visual acuity task. *Nat Neurosci* 13: 1549–1553, 2010. doi:10.1038/nn.2663.

Krauzlis RJ, Goffart L, Hafed ZM. Neuronal control of fixation and fixational eye movements. *Philos Trans R Soc Lond B Biol Sci* 372: 20160205, 2017. doi:10.1098/rstb.2016.0205.

Lachaux JP, Rodriguez E, Martinerie J, Varela FJ. Measuring phase synchrony in brain signals. *Hum Brain Mapp* 8: 194–208, 1999. doi:10.1002/(SICI)1097-0193(1999)8:4<194::AID-HBM4>3.0.CO;2-C.

Landau AN, Fries P. Attention samples stimuli rhythmically. *Curr Biol* 22: 1000–1004, 2012. doi:10.1016/j.cub.2012.03.054.

Landau AN, Schreyer HM, van Pelt S, Fries P. Distributed attention is implemented through theta-rhythmic gamma modulation. *Curr Biol* 25: 2332–2337, 2015. doi:10.1016/j.cub.2015.07.048.

Laubrock J, Engbert R, Kliegl R. Microsaccade dynamics during covert attention. *Vision Res* 45: 721–730, 2005. doi:10.1016/j.visres.2004.09.029.

Le Van Quyen M, Foucher J, Lachaux J, Rodriguez E, Lutz A, Martinerie J, Varela FJ. Comparison of Hilbert transform and wavelet methods for the analysis of neuronal synchrony. *J Neurosci Methods* 111: 83–98, 2001. doi:10.1016/S0165-0270(01)00372-7.

Lowet E, Roberts MJ, Bosman CA, Fries P, De Weerd P. Areas V1 and V2 show microsaccade-related 3-4-Hz covariation in gamma power and frequency. *Eur J Neurosci* 43: 1286–1296, 2016. doi:10.1111/ejn.13126.

Maris E, Oostenveld R. Nonparametric statistical testing of EEG- and MEG-data. *J Neurosci Methods* 164: 177–190, 2007. doi:10.1016/j.jneumeth.2007.03.024.

Martinez-Conde S, Macknik SL, Hubel DH. Microsaccadic eye movements and firing of single cells in the striate cortex of macaque monkeys. *Nat Neurosci* 3: 251–258, 2000. doi:10.1038/72961.

Montemurro MA, Rasch MJ, Murayama Y, Logothetis NK, Panzeri S. Phase-of-firing coding of natural visual stimuli in primary visual cortex. *Curr Biol* 18: 375–380, 2008. doi:10.1016/j.cub.2008.02.023.

Oostenveld R, Fries P, Maris E, Schoffelen JM. FieldTrip: Open source software for advanced analysis of MEG, EEG, and invasive electrophysiological data. *Comput Intell Neurosci* 2011: 156869, 2011. doi:10.1155/2011/156869.

Peel TR, Hafed ZM, Dash S, Lomber SG, Corneil BD. A causal role for the cortical frontal eye fields in microsaccade deployment. *PLoS Biol* 14: e1002531, 2016. doi:10.1371/journal.pbio.1002531.

Poletti M, Listorti C, Rucci M. Microscopic eye movements compensate for nonhomogeneous vision within the fovea. *Curr Biol* 23: 1691–1695, 2013. doi:10.1016/j.cub.2013.07.007.

Poletti M, Rucci M. A compact field guide to the study of microsaccades: Challenges and functions. *Vision Res* 118: 83–97, 2016. doi:10.1016/j.visres.2015.01.018.

Rolfs M, Kliegl R, Engbert R. Toward a model of microsaccade generation: the case of microsaccadic inhibition. *J Vis* 8: 1–23, 2008. doi:10.1167/8.11.5.

Song K, Meng M, Chen L, Zhou K, Luo H. Behavioral oscillations in attention: rhythmic α pulses mediated through θ band. *J Neurosci* 34: 4837–4844, 2014. doi:10.1523/JNEUROSCI.4856-13.2014.

Tian X, Chen CY. Probing perceptual performance after microsaccades. *J Neurosci* 35: 2842–2844, 2015. doi:10.1523/JNEUROSCI.4983-14.2015.

Tian X, Yoshida M, Hafed ZM. A microsaccadic account of attentional capture and inhibition of return in Posner cueing. *Front Syst Neurosci* 10: 23, 2016. doi:10.3389/fnsys.2016.00023.

Tomassini A, Spinelli D, Jacono M, Sandini G, Morrone MC. Rhythmic oscillations of visual contrast sensitivity synchronized with action. *J Neurosci* 35: 7019–7029, 2015. doi:10.1523/JNEUROSCI.4568-14.2015.

VanRullen R. Perceptual cycles. *Trends Cogn Sci* 20: 723–735, 2016. doi:10.1016/j.tics.2016.07.006.

Wang XJ. Neurophysiological and computational principles of cortical rhythms in cognition. *Physiol Rev* 90: 1195–1268, 2010. doi:10.1152/physrev.00035.2008.

Wilming N, Harst S, Schmidt N, König P. Saccadic momentum and facilitation of return saccades contribute to an optimal foraging strategy. *PLOS Comput Biol* 9: e1002871, 2013. doi:10.1371/journal.pcbi.1002871.

Wutz A, Muschter E, van Koningsbruggen MG, Weisz N, Melcher D. Temporal integration windows in neural processing and perception aligned to saccadic eye movements. *Curr Biol* 26: 1659–1668, 2016. doi:10.1016/j.cub.2016.04.070.

Yuval-Greenberg S, Merriam EP, Heeger DJ. Spontaneous microsaccades reflect shifts in covert attention. *J Neurosci* 34: 13693–13700, 2014. doi:10.1523/JNEUROSCI.0582-14.2014.

Zanos TP, Mineault PJ, Guitton D, Pack CC. Mechanisms of saccadic suppression in primate cortical area V4. *J Neurosci* 36: 9227–9239, 2016. doi:10.1523/JNEUROSCI.1015-16.2016.

Zanos TP, Mineault PJ, Nasiotis KT, Guitton D, Pack CC. A sensorimotor role for traveling waves in primate visual cortex. *Neuron* 85: 615–627, 2015. doi:10.1016/j.neuron.2014.12.043.

Zoefel B, Sokoliuk R. Investigating the rhythm of attention on a fine-grained scale: evidence from reaction times. *J Neurosci* 34: 12619–12621, 2014. doi:10.1523/JNEUROSCI.2134-14.2014.

Zuber BL, Stark L. Saccadic suppression: elevation of visual threshold associated with saccadic eye movements. *Exp Neurol* 16: 65–79, 1966. doi:10.1016/0014-4886(66)90087-2.

Zuber BL, Stark L, Cook G. Microsaccades and the velocity-amplitude relationship for saccadic eye movements. *Science* 150: 1459–1460, 1965. doi:10.1126/science.150.3702.1459.